PHYSICAL AND ANALYTICAL PROPERTIES OF A MICROWAVE EXCITED PLASMA

By

KAREN FALLGATTER

A DISSERTATION PRESENTED TO THE GRADUATE COUNCIL OF
THE UNIVERSITY OF FLORIDA
IN PARTIAL FULFILLMENT OF THE REQUIREMENTS FOR THE
DEGREE OF DOCTOR OF PHILOSOPHY

UNIVERSITY OF FLORIDA
1970

ACKNOWLEDGMENTS

The author is grateful to her research director, Dr. J. D. Winefordner, for his help and guidance in all phases of her work at the University of Florida. She also appreciates the advice of Dr. Vratislav Svoboda.

She thanks the United States Air Force for providing the funds which supported her research.

Special appreciation goes to Michael for his patience, understanding and encouragement.

TABLE OF CONTENTS

Page

ACKNOWLEDGMENTS ii

LIST OF TABLES. v

LIST OF FIGURES vi

ABSTRACT. viii

CHAPTER

I. INTRODUCTION. 1

II. THEORETICAL CONSIDERATIONS. 12

- Equilibrium in plasmas 12
- Deviation from equilibrium in plasmas. . . . 13
- Determination of temperature from spectral lines 15
- Determination of temperature from band systems of diatomic molecules. 20
- Determination of electron density from Stark broadening of the hydrogen Balmer lines 22
- Determination of the radial distribution of emitters from the axial distribution 25

III. INSTRUMENTAL AND EXPERIMENTAL 31

- Optics 31
- Readout. 33
- Aerosol and gas. 35
- Early cell designs 37
- Initiation of the plasma 40
- Adjustment of optics 41
- Monochromator calibration. 42
- Measurement of the spectral bandwidth. . . . 45
- Measurement of signals of argon lines. . . . 48
- Measurement of signals of lines of the 0,0 band of the $^2\Pi \rightarrow {}^2\Sigma$ OH system 49

CHAPTER Page

Measurement of the profile of the hydrogen beta line 49
Measurement of the axial signal profile of the plasma. 50
Analytical curves 51
Calibration of the micrometer screw 52

IV. RESULTS AND DISCUSSION 53

Appearance and spectra of the plasma. . . . 53
Temperature measurements in the plasma. . . 56
Electron density measurements 73
Summary of plasma properties. 76
Analytical results. 80

BIBLIOGRAPHY 88

BIOGRAPHICAL SKETCH. 91

LIST OF TABLES

Table Page

1. Wavelengths, Energies and Transition Probabilities for Argon Lines Used in Temperature Determinations 58

2. Wavelengths, Energies and Transition Probabilities for the Rotational Lines of the Electronic Band System of OH Used in Temperature Determinations 61

3. Properties of the Microwave Discharge Through Argon. 77

4. Wavelengths, Detection Limits and Standard Deviations for Five Elements 83

5. Properties of the Part of the Discharge Used for the Analytical Curves. 86

LIST OF FIGURES

Figure		Page
1.	Calculated profile of the hydrogen beta line for a temperature of 5000 K and an electron density of 10^{15} cm^{-3}	24
2.	Relationship between the full Stark width at half maximum and the electron density for a temperature of 5000 K.	26
3.	Relationships used in the transformation of axial distributions into radial distributions.	28
4.	Schematic diagram of the optical and electrical system of the apparatus	32
5.	Quartz cell used to contain the plasma	34
6.	The dry aerosol producing system	36
7.	Relative calibration curves for the tungsten strip lamp and the optical system.	43
8.	Slit function of the Heath monochromator . . .	47
9.	The background spectrum of the plasma from 2400 to 4100 Å	54
10.	The background spectrum of the plasma from 4100 to 5600 Å	55
11.	Spectrum of part of the OH 0,0 band system . .	57
12.	Logarithmic plots for argon lines for two plasma conditions.	60
13.	Logarithmic plots for OH lines for two plasma conditions	63
14.	Observed and transformed plasma signal profiles for the 4259.1 Å line of argon. . . .	65

Figure Page

15. Observed and transformed plasma signal profiles for the 4266.3 Å line of argon. . . . 66

16. Observed and transformed plasma signal profiles for the 4272.2 Å line of argon. . . . 67

17. Observed signal profiles of the plasma for the $Q_1(6)$, $Q_1(9)$ and $Q_1(13)$ lines of the 0,0 OH band 68

18. Transformed signal profiles of the plasma for the $Q_1(6)$, $Q_1(9)$ and $Q_1(13)$ lines of the 0,0 OH band. 69

19. Relationship between the radiance of the argon 4259.4 Å line and the temperature. 71

20. Temperature profiles in the plasma for two plasma conditions. 72

21. Observed profile of the hydrogen beta line . . 74

22. Variation of electron density with position in the plasma. 75

23. Analytical curves for indium and gallium . . . 81

24. Analytical curves for mercury, cadmium and zinc 82

25. Change of signal with distance from the center of the plasma for the plasma background and for zinc emission. 85

Abstract of Dissertation Presented to the Graduate
Council in Partial Fulfillment of the Requirements
for the Degree of Doctor of Philosophy

PHYSICAL AND ANALYTICAL PROPERTIES OF A MICROWAVE EXCITED PLASMA

By

Karen Fallgatter

August, 1970

Chairman: James D. Winefordner
Major Department: Chemistry

A microwave generator with a maximum power output of 120 watts was used to sustain a discharge through flowing argon at atmospheric pressure, using a tapered rectangular cavity to couple the microwave power into the plasma discharge. A cell constructed from fused quartz tubing was used to contain the plasma, which was about 6 cm long and 0.05 cm in diameter. Excitation temperatures in the plasma were determined by applying the logarithmic plot method and the absolute radiance method to the measured radiances of argon atomic lines. At the center of the plasma, the logarithmic plot method gave a temperature of 6280 K, while a temperature of 8520 K was obtained using the absolute radiance method. The radiances of some rotational lines of

the OH electronic band system were used to determine rotational temperatures by the logarithmic plot method. A rotational temperature of 2440 K was obtained at a point 0.08 mm from the center of the discharge. The width at half maximum of the Balmer hydrogen beta line was measured at several locations in the discharge. The Stark broadening of the hydrogen line was then used in the calculation of the electron density in the plasma. An electron density of 2.6×10^{15} cm^{-3} was obtained at the center of the plasma.

The Abel transform was applied to the axial radiances from the non-homogeneous plasma. The resulting radial radiances for argon lines yielded, using the absolute radiance method, a temperature of 9010 K at the center of the plasma. The transform shows that in the center of the plasma, emission from OH is negligible.

The plasma was examined as a source of excitation in atomic emission spectrometry. A dry aerosol, produced by a system consisting of a pneumatic sprayer which nebulized 1.1 ml/min of aqueous sample solution, a heated chamber and a specially constructed condenser, could be introduced into the plasma. Analytical curves were obtained and detection limits estimated for cadmium, gallium, indium, mercury and zinc. Atomic lines of calcium, strontium, lead and boron were observed, but no analytical curves were determined. A position in the plasma cell at a distance of about 0.3 mm from the center of the plasma was found to give the best analytical results for most of the elements examined. At this position, the absolute radiance of an argon line indicated a temperature of 4920 K and the two line method for lines of calcium and strontium yielded temperatures of 4980 and 5050 K respectively. A value of 1.8×10^{15} cm^{-3} was obtained for the electron density in the analytical region.

CHAPTER I

INTRODUCTION

In the last decade, the properties and uses of several kinds of high temperature plasmas have been the subject of a great deal of research. The definition of plasma is very broad and is considered to include any electrically conductive gaseous system which is at least partially ionized. Consequently, the designation of plasma is applied to phenomena as varied as the ionosphere and the exhaust of rockets as well as to the various electrical discharge plasmas utilized in emission spectroscopy.

Electrical discharge plasmas have been employed by chemists and physicists both in the spectroscopic study of excited plasma gases and as a source of energy for the excitation of other materials. For the past few decades, the electric arc, which is the plasma region between conducting electrodes, has been one of the most widely used methods of exciting the spectra of metals for the purpose of chemical analysis. However, the arc is spatially unstable, which generally restricts the methods of observing the emission signals to those such as the photographic method which integrate the signals. Another problem with the arc is that electrodes must be used. The electrode material is eroded by the arc and is then a contaminant in the arc.

The idea of using a high frequency discharge as a spectrographic source was introduced by Gatterer [1]. This type of plasma, which is sometimes referred to as the electrodeless discharge, can have energy coupled into it without the use of internal electrodes. Radio frequency and microwave generated plasmas also have the advantage of being able to reach extremely high excitation temperatures. This property of these plasmas makes it possible to observe emission from such hard to excite elements as boron, titanium and tungsten.

Gatterer introduced samples containing halogens, sulfur or selenium into glass tubes which were then evacuated. The spectra of these elements were then observed in an electrodeless discharge in the evacuated tubes. In 1954, Mavrodineanu and Boiteux [2] suggested that the high frequency plasma studied by Cristescu and Grigorovici [3] should be useful as an excitation source. This plasma, a radio frequency discharge through a diatomic gas, was employed analytically by Bădărău and associates [4], who used a pneumatic sprayer to introduce sample solution.

In 1963, Mavrodineanu and Hughes [5] studied the analytical capabilities of two plasma torches. One was powered by a 250 W triode driven oscillator at 30 MHz. In this plasma, the discharge originated at a conical tip at the end of a conductor which formed part of the tank circuit. A gas stream of hydrogen or helium which carried the aspirated sample exited from small holes in the discharge tip. The second plasma torch was powered by a 2 kW magnetron at 2450 MHz. The discharge was established at the conical tip which terminated the center conductor of a coaxial coupling device. Solid samples were introduced into the discharge in graphite cup electrodes. Both of the plasma torches were used in conjunction with a spectrograph, and the spectra of about seventy elements were photographed.

Another plasma torch coupled by a tank circuit was investigated by West and Hume [6]. Power was provided by a 500 W 27 MHz generator and nitrogen was the plasma gas. An ultrasonic nebulizer system was used to introduce aqueous samples into the nitrogen stream. The emission from the plasma was monitored photometrically. Detection limits, which compared rather favorably with limits obtained by flame emission, were obtained for twenty one elements. Also, a few checks for sample matrix effects indicated no interference. For example, one hundred-fold excesses of aluminum and phosphate had no effect on the emission signals of calcium and strontium.

In 1964, Greenfield, Jones and Berry [7] studied an induction-coupled plasma powered by a 36 MHz generator with an output of 1.5 kW as an emission source for both a spectrograph and a spectrophotometer. Argon flowed through the discharge region at a rate of 5 l/min and a flow of 17 l/min of argon was used to cool the walls of the cylindrical discharge chamber. The aqueous sample was nebulized through the low temperature region in the center of the toroidal discharge. Eight elements were investigated for detection limits. Neither aluminum nor phosphate was found to cause a change in the emission signal for calcium. The temperature of the plasma was found to be 12,000 to 15,000 K in the maximum field region and about 8,000 K in the tail flame.

A few years later, Greenfield *et al*. [8] found that the length of the induction coupled plasma could be increased to about two feet. They also discovered that the plasma could be bent through a right angle and that the tail flame of the plasma could be split. Use of these properties resulted in a T-shaped plasma which provided the long path length desirable for atomic absorption measurements. Greenfield and co-workers used this form of the plasma both as an absorption cell and as an emission source for atomic absorption measurements in an air/acetylene flame.

Wendt and Fassel [9] investigated an induction-coupled plasma similar to that of Greenfield. Their system was operated at 3.4 MHz with powers up to 5 kW. A flow of 20 l/min of argon was used to cool the walls of the quartz tube containing the discharge while 0.4 l/min were used to maintain the discharge and 0.5 l/min served to carry the aerosol formed by an ultrasonic nebulizer into the plasma. Detection limits for atomic emission were run for twenty elements. The tear-shaped plasma exhibited strong atomic lines of argon, but only two faint argon ion lines were found.

In later work, Wendt and Fassel [10] used the same induction-coupled plasma system to determine the detection limits of nine elements by atomic absorption. A multiple pass mirror assembly was used to increase the path length. Checks for aluminum and phosphate interference with the determination of calcium indicated that a slight increase in absorption occurred for ratios of interferent to calcium greater than about five.

Fassel and Dickinson [11,12] found that increasing the frequency of the generator from the 3.4 MHz used by Wendt and Fassel to 30 MHz changed the shape of the discharge from tear-shaped to toroidal. This toroidal shape proved to be an advantage because of a sample introduction problem peculiar to plasmas. Aerosol and powdered samples tend to be reflected from or pass along the outer surfaces of induction-coupled plasmas. However, samples can be introduced into the relatively cool hole in the toroid with far less resistance. This improvement in sample introduction led to substantial improvements in detection limits compared to those given in reference [9]. Data were given for twenty six elements with detection limits ranging from 0.12 mg/ml for antimony to 0.00002 mg/ml for strontium.

The induction-coupled torch used by Veillon and Margoshes [13] was operated at 4.8 MHz with a maximum power of 5 kW. A nebulization system producing a dry aerosol [14] was used for sample introduction. Detection limits for nine elements were found by both atomic emission and atomic absorption. The effects of aluminum and phosphate concentrations on the emission signal of calcium were investigated. In contrast to the results of other workers [6,9] Veillon and Margoshes observed considerable enhancement of calcium emission signal with increasing aluminum concentration. A smaller enhancement was observed for phosphate.

A 900 W, 2450 MHz microwave generator was used by Goto, Hirokawa and Suzuki [15] to power a nitrogen plasma torch. They employed a chamber type nebulizer to introduce sample into the plasma. Analytical curves for four elements and detection limits for seventeen elements were obtained.

The temperature distribution of the plasma was studied by observing the radiances of iron lines. The maximum temperature was 4,500 K.

A discharge was generated at the open end of a coaxial wave guide by a 520 MHz, 200 W generator in work done by Yamamoto and Murayama [16]. An argon flow of 6.5 l/min was used to nebulize aqueous samples and maintain the discharge. The stability of emission of the system was investigated, and detection limits were run for six elements. The absolute intensity of the argon 4159 Å line was used to determine the excitation temperature of the plasma. On the central axis of the plasma, the excitation temperature was 8,150 K.

In 1968, Murayama, Matsumo and Yamamoto [17] used a 2450 MHz, 400 W discharge in argon for the excitation of metal spectra. As in earlier work [16], the discharge was generated at the open end of a coaxial line wave guide and the argon flow rate was again 6.5 l/min. It was observed that while the radiances of argon lines were greatest in the core of the discharge, the lines of metals exhibited greater radiances in the outer zone of the plasma. These researchers also noticed that the addition of sodium chloride to the sample solutions resulted in fairly large increases in the emission signals of several metals. Twenty five elements were investigated for detection limits.

The absolute radiance of the hydrogen β line indicated a temperature of 6,400 K.

Recently, Murayama [18] used the same system described in reference [17] to investigate the emission of rare earth elements. In this study, the addition of 1,000 ppm of sodium was found to improve the detection limits of rare earth elements by about two orders of magnitude. Measurements of the emission signal due to the samarium ion line at 4424 Å were made for several sodium concentrations and at several positions in the plasma. The addition of 1,000 ppm of sodium to the plasma was found to reduce the temperature from 6,900 K to 6,600 K and to decrease the electron density from 2×10^{14} cm^{-3} to 1×10^{14} cm^{-3}. Another advantage of adding sodium noted by these authors was that the working curve of neodymium with 1,000 ppm of sodium added is linear while, when sodium is not added, the log signal versus log concentration plot increased in steepness with increasing concentration. For an increase in concentration from 500 ppm to 1,000 ppm, the signal increased by a factor of six. Murayama attributes the interelement effects to changes in the mass transport and degree of ionization.

Another use of the microwave discharge in argon was made by McCormack, Tong and Cooke [19]. They used a 2450 MHz generator at powers from 20 to 125 W to excite molecules in the argon carrier gas of a gas chromatographic system. The gas was allowed to flow through a quartz tube placed in the slot of a tapered rectangular cavity. Organic molecules in the argon stream were fragmented and the resulting diatomic molecules and atoms were excited by the electrons in the microwave discharge. Subsequently, Lisk and co-workers [20,21,22] used this detector in work on insecticides and insecticide residues. Use of plasmas for gas analysis under low pressure conditions has been reported by several researchers [23,24,25,26].

In 1967, Runnels and Gibson [27] used a low wattage microwave plasma to excite metals. A cavity of the Evenson design was used to couple the microwave energy into a discharge occurring in atmospheric pressure argon. The 2450 MHz microwave generator used had a power output of up to 100 W, but was generally used at 25 W. Samples were deposited on a platinum filament which was then placed in the discharge cell and heated to a temperature high enough to completely evaporate the sample. Analytical curves and detection limits were run for six elements and studies were made on sample matrix effects. Heating of the argon prior to its entry into the discharge was observed to lower the signals due to atom and ion emission, but to raise the level of the background continuum.

Another system for vaporizing samples into an argon plasma was described by Kleinmann and Svoboda [28]. These workers used a 40 MHz 200 W generator coupled through a coil to maintain the discharge. Sample was introduced into the system by applying solution to a graphite disk in the discharge chamber. After the discharge was initiated, the sample was vaporized by resistance heating. Limits of detection for fifteen elements were run on this system.

The foremost problem encountered by workers investigating the analytical applications of atmospheric pressure plasmas has been that of sample introduction. Most of the plasmas used had a low tolerance for water vapor, so either the rate of nebulization had to be low or a method of desolvating the aerosol had to be employed.

In spite of the sample introduction problem, radio frequency and microwave plasmas should be better than chemical flames for the excitation of metal spectra. When flames are used, two serious problems are encountered. First, the relatively low temperature causes a low atomization efficiency for some molecules introduced into a flame. A second problem which is a very serious limitation of flames is compound formation of the analyte atoms with flame gas products, for example, O, OH and H. The temperature of a plasma is higher than that of a chemical flame, so the atomization efficiency is also higher and compound formation in an inert gas plasma is minimal. Thus, if the problems of getting samples into plasmas can be overcome, plasmas should be much better than flames for the excitation of metal spectra.

CHAPTER II

THEORETICAL CONSIDERATIONS

Equilibrium in plasmas

In order for a plasma to be in a state of complete thermodynamic equilibrium, it must be homogeneous and have an optical thickness which is large compared to one. The optical thickness for a homogeneous plasma is given by

$$\tau(\nu) = k(\nu)\ell \qquad (1)$$

where $k(\nu)$ is the absorption coefficient per cm and ℓ is the thickness of the emitting layer in centimeters. Most plasmas, however, are optically thin, that is $\tau(\nu) \leqq 1$, so that complete thermodynamic equilibrium cannot exist. This prevents the total description of the state of the plasma by a few thermodynamic variables, because rate processes are also involved. On the other hand, spectroscopic analysis is only possible on an optically thin plasma. In an optically thick plasma no radiation from the plasma interior can be measured.

The state of local thermodynamic equilibrium (LTE) [29,30] is close to the state of complete thermodynamic equilibrium and is often observed for the plasma state.

The designation LTE is given to that state in which all distributions except that of the radiation energy are given by the Boltzmann distribution. Here, the temperature, T, in the Maxwell-Boltzmann velocity distribution is identical to T in the Maxwell-Boltzmann internal energy distribution, equation (4), and to T in the Saha equation (9). The spectral radiance, B, however, is not identical to the black body radiance $B_\lambda(T)$. More detailed discussions of LTE and the conditions under which it occurs may be found in two papers by Bates, Kingston and McWhirter [31,32] and in references [29] and [30].

Deviation from equilibrium in plasmas

References [29], [30] and [33] also describe several categories of non-LTE plasmas. One case, of interest here, is that of plasmas heated by electrons [30], in which electrons continuously gain surplus energy from the electrical field. As a result of the continuous energy gain, only a partial transfer of surplus energy from the electrons to the atoms in the plasma is possible. Thus, equilibrium is never reached, but a steady state is attained in which the difference between the electron temperature and the gas temperature is equal to the energy gain from the field. The relative difference in temperature is given by [33]:

$$\frac{T_e-T_g}{T_e} = \frac{(eE)^2}{(\frac{3}{2}\ kT_e)^2}\ \frac{m}{4m_e} \qquad (2)$$

where λeE is the energy which is acquired by an electron from the electrical field E as it travels one mean free length of path and $\frac{3}{2}\ kT_e$ is the thermal energy of the electrons. In equation (2), T_e is the electron temperature, T_g is the gas temperature, e is the charge on the electron, λ is the mean free path, E is the field strength, m is the mass of the atomic species in the plasma, and m_e is the mass of the electron. At atmospheric pressure, the mean free path is of the order of 10^{-5} cm, so that the temperature difference is small for commonly used electrical field strengths. For a discharge in atmospheric pressure argon at T_e = 8000 K and E = 20 V/cm, the temperature difference is 10 K.

Another category of non-LTE plasma is one in which the electron density falls below a certain critical value (in an argon plasma, LTE occurs at $n_e = 5 \times 10^{15}$ cm^{-3} [34]). Such a plasma is said to be in partial local thermodynamic equilibrium [29,30]. This state has been shown by McWhirter and Hearn [35] to involve the overpopulation of ground states. However, for all collisional processes which do not involve atoms in the ground state, detailed balancing holds.

Determination of temperature from spectral lines

The spectral line of wavelength λ_{qp} resulting from a transition between an upper level, q, and a lower level, p, has a radiance, B, given by:

$$B = c\ell A_{qp} n_q h/4\pi\lambda_{qp} \tag{3}$$

where B has units of watts/cm^2-steradian, c is the velocity of light in cm/sec, ℓ is the thickness in cm of the emitting region, n_q is the number density in atoms/cm^3 of atoms in state q, A_{qp} is the transition probability in sec^{-1} of a transition from state q to state p, h is Planck's constant in erg-sec, and λ_{qp} is the wavelength in centimeters.

For a Maxwell-Boltzmann distribution,

$$n_q = \frac{ng_q}{Q} \exp(-E_q/kT) \tag{4}$$

where n is the total number density of atoms or ions of the emitting species, g_q is the degeneracy of state q, Q is the electronic partition function, E_q is the energy in ergs of level q, k is the Boltzmann constant in ergs/deg, and T is the temperature in degrees K. Then, by combining equations (3) and (4):

$$B = \frac{c\ell A_{qp} g_q nh}{4\pi\lambda_{qp} Q} \exp(-E_q/kT) \tag{5}$$

is obtained.

Rearrangement of equation (5) in logarithmic form gives:

$$\log \left(\frac{B\lambda_{qp}}{g_q A_{qp}}\right) = \log \frac{c\ell nh}{4\pi Q} - (E_q/kT)\log e \quad . \tag{6}$$

Evaluation of the constants in equation (6) yields:

$$\log \left(\frac{B\lambda_{qp}}{g_q A_{qp}}\right) = \log \frac{\ell n}{Q} - \frac{0.62486E_q}{T} - 16.801 \quad . \tag{7}$$

For the determination of temperature from the radiance of a single line, the partition function, Q, which is defined by

$$Q = \sum_q g_q \exp(-E_q/kT) \tag{8}$$

must be known. de Galan, Smith, and Winefordner [36] have calculated partition functions for seventy three elements over a temperature range between 1,500 and 7,000 degrees K.

The usual method of applying equation (7) is to prepare a plot of B versus temperature for each line to be used. Values of λ_{qp}, g_q E_q and Q are obtained from published tables, but accurate values of A_{qp} are known for relatively few lines. Fortunately, B is much more dependent on the temperature than on the transition probability. The number density, n, of neutral atoms is a function of temperature. For a gas consisting of a single species at temperatures where ionization is negligible, the ideal gas law can be used to calculate the number density. For temperatures at which ionization is appreciable, the Saha equation of ionization equilibrium,

$$\frac{n_+ n_e}{n} = \frac{(2\pi mkT)^{3/2}}{h^3} \; \frac{Q_+ Q_e}{Q} \; \exp(-E_i/kT) \; , \qquad (9)$$

must be used to determine the number density. In equation (9), n_+ is the ion number density, n_e is the electron number density, n is the neutral atom number density, Q_+ and Q are the partition functions of the ion and atom, Q_e is the electron partition function ($Q_e = 2$), and E_i is the ionization energy. The determination of n for a species becomes more difficult if the gas consists of more than one species, because a system of simultaneous equations must then be solved to determine the number densities of all the neutral species and the temperature T. The path length, ℓ , is measured by scanning the optical path laterally across the emitting gas to determine the points at which the radiance falls to a negligible value. The distance between these points is ℓ .

It is apparent that the application of the absolute radiance method of determining temperature, that is, the application of equation (7), may be somewhat difficult if values of the partition functions are not available for the desired temperature range or if the emitting gas contains several species. Also, the lack of accurate absolute transition probabilities leads to errors in the results.

However, it is not necessary to know the number density, partition function, or path length in order to use the two line radiance ratio method. For two lines of the same species having the same lower state, equation (5) can be used to yield:

$$\frac{B_1}{B_2} = \frac{g_1 A_1 \lambda_2}{g_2 A_2 \lambda_1} \exp(-(E_1 - E_2)/kT) \qquad (10)$$

where the subscripts refer to the two spectral lines. An additional advantage of this method is that relative transition probabilities can be used. Relative transition probabilities are available for many elements for which reliable absolute transition probabilities are not known.

The logarithmic plot method, which is the extension of the two line method to many lines, may also be used to determine the temperature. For this method, equation (7) takes the form:

$$\log(B\lambda_{qp}/g_q A_{qp}) = C - \frac{E_q}{kT} \log(e) \qquad (11)$$

where $C = \log(c\lambda nh/4\pi Q)$. A plot of $\log(B_{qp}\lambda_{qp}/g_q A_{qp})$ versus $E_q \log(e)/kT$ results in a straight line having a slope of $-1/T$. Use of the logarithmic plot reduces the possibility of an error in temperature due to a choice of a bad line, that is, a line which is overlapped by another line, or a line which is self-absorbed. In equations (8) and (11), a "bad" line can cause substantial error.

Use of an atom line and an ion line from the same species may also be made in order to determine temperature. From equation (5):

$$\frac{B_+}{B} = \frac{g_+A_+\lambda}{gA\lambda_+} \quad \frac{n_+}{n} \quad \frac{Q}{Q_+} \exp(-(E_+-E)/kT) \qquad (12)$$

where the subscript + indicates the ion. Combining equations (9) and (12) gives

$$\frac{B_+}{B} = \frac{g_+A_+\lambda}{gA\lambda_+} \quad \frac{Q_e}{n_e} \quad \frac{(2\pi mkT)^{3/2}}{h^3} \exp(-(E_+-E+E_i)/kT) \; . \qquad (13)$$

Because $Q_e = 2$,

$$\frac{B_+}{B} = 9.66 \times 10^{15} \frac{g_+A_+\lambda}{gA\lambda_+} \frac{T^{3/2}}{n_e} \exp(-1.4388(E_+-E+E_i)/kT) \qquad (14)$$

where E_+, E, and E_i are expressed in cm^{-1}. In logarithmic form, equation (14) becomes

$$\log(\frac{B_+}{B}) = \log \frac{g_+A_+\lambda}{gA\lambda_+} - \log(n_e) + \frac{3}{2}\log(T) + 15.985 - \frac{0.62486}{T}(E_+-E+E_i) \; . \qquad (15)$$

Because the difference in energy between E_i and E is usually larger than the difference in energy of two neutral atom lines of the same species, equation (15) tends to yield a more accurate temperature than does equation (10), providing that accurate values of the electron density are available.

In addition to the sources of error mentioned above, deviations from a Maxwell-Boltzmann distribution in a non-LTE source lead to errors in temperature determinations.

Determination of temperature from band systems of diatomic molecules

The rotational radiance distribution in the fine structure of a band of a diatomic molecule may be utilized in the determination of effective rotational temperatures. For a rotational transition, the radiance due to a transition from state J to J' is given by

$$B = C_1 n_J A_{JJ'} h\nu_{JJ'} \qquad (16)$$

where C_1 is a constant including parameters from the measuring apparatus, n_J is the number of molecules in state J, $A_{JJ'}$ is the transition probability, and $\nu_{JJ'}$ is the frequency of the transition. The number of molecules in state J is given by:

$$n_J = \left(\frac{n}{Q_R}\right) (2J+1) \exp(-\bar{B}\, J(J+1)hc/kT) \qquad (17)$$

where n is the total number of molecules, Q_R is the rotational partition function, and B is the rotational constant, in cm^{-1}, for the upper state. Combining equations (16) and (17) yields,

$$B = C_1 A_{JJ'} h\nu(\frac{n}{Q_R}) (2J+1) \exp(-BJ(J+1)hc/kT) \quad . \qquad (18)$$

If $C_2 = C_1 h$ and $E_R = \bar{B} J(J+1)hc$, equation (18) becomes

$$B = C_2 A_{JJ'} \nu(\frac{n}{Q_R}) (2J+1) \exp(-E_R/kT) \quad . \qquad (19)$$

The logarithmic form of equation (19) is:

$$\log(B) = \log(C_2 n/Q_R) + \log(A_{JJ'} \nu(2J+1)) - \frac{E_R}{2.303kT} \qquad (20)$$

or, letting $A_{JJ'}(2J+1) = A'$ and $C_3 = \log(C_2 n/Q_R)$,

$$\log(B/A'\nu) = C_3 - E_R/2.303kT \, . \qquad (21)$$

Equation (21) is the form used in the atomic logarithmic plot method. The values for $\log(B/A'\nu)$ are plotted versus the energies of the upper state, E_R, and the slope of the resulting line is $-1/2.303kT$.

Another method of determining temperature from rotational lines is the iso-intensity method which is favored by Dieke and Crosswhite [37]. This method makes use of the fact that, for a branch, the radiance at first increases with increasing rotational quantum number, then reaches a maximum and decreases again. As a result of this distribution, it is possible to select two lines of the same radiance, one weak line near the beginning of the branch and another line toward the end of the same branch.

It may be necessary to interpolate between lines, so that a line of equal radiance may be one of non-integral quantum number. If the two lines are denoted by subscripts 1 and 2, equation (21) gives

$$\frac{E_{R_1} - E_{R_2}}{2.303kT} = \log(A_1, \nu_1) - \log(A_2, \nu_2) \qquad (22)$$

which may be used to calculate the temperatures. The advantage of using the iso-intensity method is that the self-absorption is nearly equal for lines of equal radiance. Thus, the iso-intensity method is only slightly affected by self-absorption while in the molecular logarithmic plot method, the observed radiance of strong lines may be too small, resulting in an erroneous temperature. On the other hand, the iso-intensity method is more affected by overlapping of lines because only a few lines are measured.

Determination of electron density from Stark broadening of the hydrogen Balmer lines

Emitting atoms and ions in a plasma are under the influence of electrical fields produced by fast-moving electrons and slow-moving ions. The general reaction law, $\Delta\nu = C/r^n$, where $\Delta\nu$ is the half width in frequency units, C is a constant and r is the perturbation distance, describes the pressure broadening of spectral lines emitted from a plasma. Different values of n are used for different types of interactions. The linear Stark effect, corresponding to n=2, and the quadratic Stark effect, for which n=4, are produced by the electrical fields of both ions and electrons. The largest broadenings are shown by hydrogen lines because broadening effects are strongest for atoms exhibiting linear Stark effects [38]. Griem, Kolb, and Shen [39,40] have calculated the line profiles of the hydrogen Balmer lines for several temperatures and electron pressures. Values given by Griem [30] for the Balmer hydrogen β line, for a temperature of 5,000 K and an electron density of 10^{15} cm^{-3} have been plotted in Figure 1. The inset in the figure shows the Stark splitting of this line. The line profile is described by a distribution function, $S(\alpha)$, and is normalized to $\int_{-\infty}^{\infty} S(\alpha)d\alpha = 1$. The value of α is given by $\alpha = \Delta\lambda/F_o$ where $\Delta\lambda$ is the half width in wavelength units of one wing of the line of wavelength λ_o and F_o is the field strength. The field strength is given by

$$F_o = \frac{2.61e}{4\pi \ _o} n_e^{2/3} \qquad (23)$$

where e is the charge on the electron in e.s.u., n_e is the electron density in cm^{-3}, and $_o$ is the dielectric constant of a vacuum.

Griem [30] has represented the electron density by:

$$n_e = C(n_e,T)\Delta\lambda_s^{3/2} \qquad (24)$$

where $\Delta\lambda_s$ is the full Stark width at half the maximum and

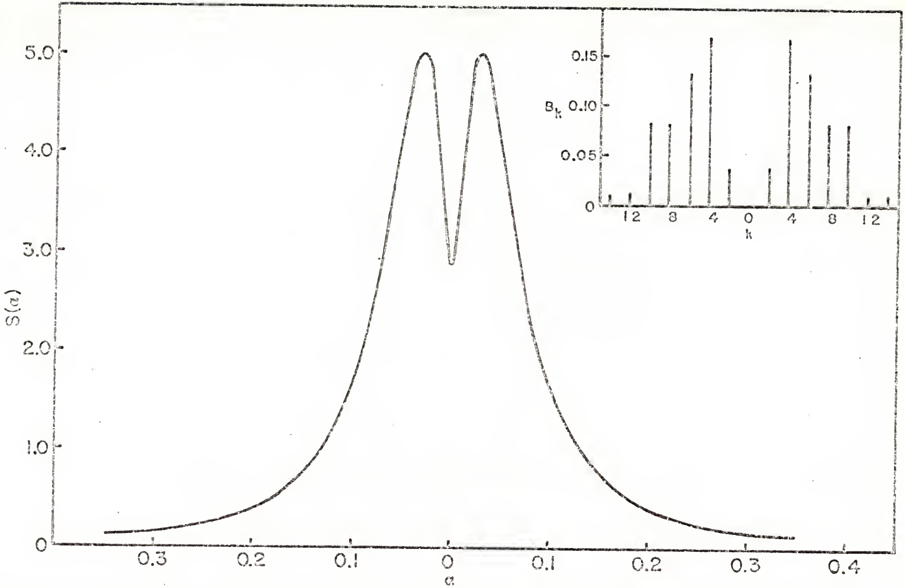

Fig. 1.-Calculated profile of the hydrogen beta line for a temperature of 5000 K and an electron density of 10^{15} cm^{-3}.

$C(n_e,T)$ is a coefficient which is weakly dependent on n_e. Also, Griem has graphically interpolated the profiles described by $S(\alpha)$ in order to determine values of the $C(n_e,T)$ coefficients and has presented the values in table form [30] for several lines, at a number of electron densities and temperatures.

The simplest way of making use of equation (24) is to make a plot of the logarithm of $\Delta\lambda_s$ versus the logarithm of n_e for a single temperature. This has been done in Figure 2 for a temperature of 5,000 K. The result is a line which curves only slightly. Temperature has a very small effect on $C(n_e,T)$ so that an accurate knowledge of the temperature is not necessary. The use of the 5,000 K curve would cause an error of less than 1 per cent if applied to the hydrogen β line profile for 10,000 K. Thus, relatively accurate determinations of electron density can be made by experimentally recording the profile of a hydrogen line, and then measuring the width of the profile at a point halfway between the baseline and the profile maximum (see Fig. 1).

Determination of the radial distribution of emitters from the axial distribution

Radiant energy from a number of layers is detected when an optical system is used to observe a source of finite volume. For a non-homogeneous plasma, each layer of plasma

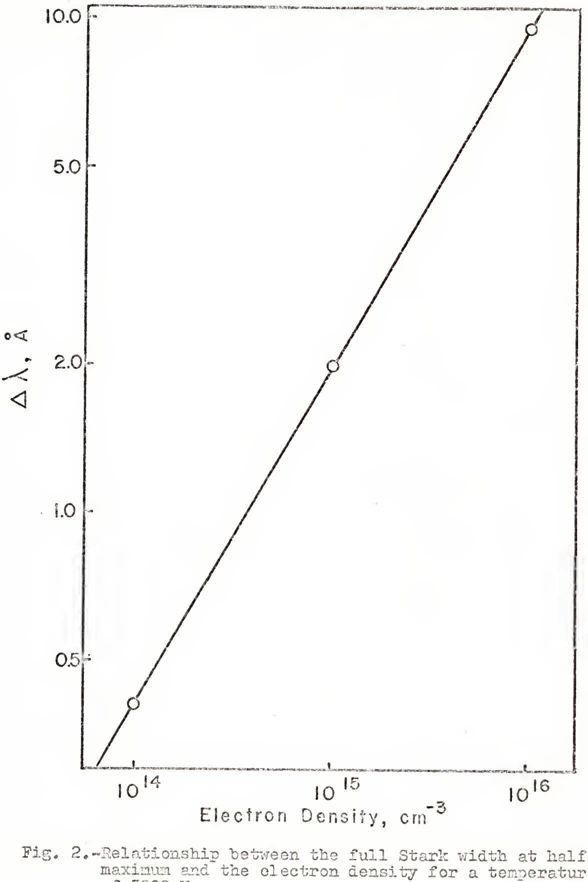

Fig. 2.-Relationship between the full Stark width at half maximum and the electron density for a temperature of 5000 K.

has an individual temperature, electron density, emissivity and thickness. Thus, the observed radiance from such a non-homogeneous source is a summation of the radiances coming from the layers.

If, as is common, the light source has cylindrical or spherical symmetry, the total radiance obtained by spatial scanning of the source can be transformed into the radial distribution within the emitting region [41,42,43]. Consider a narrow slice of the light source (see Fig. 3), taken at a distance y from the axis of the cylinder, and having a width δy and a height ℓ. A detector equipped with slits such that only the radiation that originates within the slice reaches the detector will observe a total flux given by:

$$B(y)\ell\delta y = \ell\delta y \int_{-X}^{X} f(r)dx \quad . \qquad (25)$$

Under these conditions, the part of the flux originating in the volume element $\ell dx\delta y$ is $f(r)\ell dx\delta y$. In equation (25), the integral is taken for a constant y, $x^2 + y^2 = r^2$, and $X^2 = R^2 - y^2$ where the radius beyond which f(r) is negligible is designated R. Thus equation (25) can be rewritten:

$$B(y) = 2 \int_{y}^{R} \frac{f(r)dr}{(r^2-y^2)^{1/2}} \quad . \qquad (26)$$

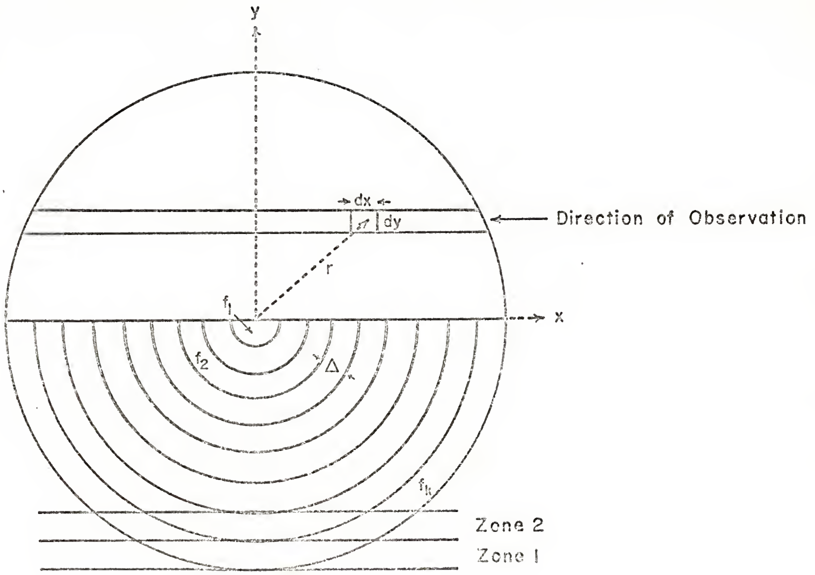

Fig. 3.-Relationships used in the transformation of axial distributions into radial distributions.

Equation (26) is one form of the Abel integral equation. The Abel inversion of equation (26) is

$$f(r) = -\frac{1}{\pi}\int_{y}^{R}\frac{(dB/dy)dy}{(y^2-r^2)^{1/2}} \tag{27}$$

where B(y) is zero for all values of r greater than R. In the application of equation (27), the y-axis and r are divided into small equal increments, Δ, so that $y_n = n\Delta$, $r_k = k\Delta$, and $R = N\Delta$ where n and k are integers from zero to N, and R is the boundary radius of the emitter.

In practice, B(y) is not obtained as an analytical function, but rather as a set of numerical data, so a numerical solution of equation (27) is desired. Kjell Bockasten [43] developed a method for the numerical solution, but, in his method, small errors in the measured values of B are amplified when the derivative of B(y) is evaluated unless the data are smoothed by some technique prior to the calculation. Another numerical method, which was developed by W. L. Barr [42], accomplishes the smoothing in the same step as the evaluation of the derivative of B(y). In Barr's method, the equations evaluated are:

$$f_k = \frac{1}{\pi\Delta}\sum_{n=k-2}^{N} \beta_{kn}B_n \qquad (k\ 2) \tag{28a}$$

$$f_k = \frac{1}{\pi\Delta}\sum_{n=0}^{N} \beta_{kn}B_n \qquad (k\ 2) \tag{28b}$$

where the weighting factors β_{kn} are functions only of k and n. A table of β values for N=20 is also given by Barr [42].

CHAPTER III

INSTRUMENTAL AND EXPERIMENTAL

Optics

A schematic diagram of the optical system is shown in Figure 4. Light from the plasma cell was focussed by a 40° off-axis toroidal mirror (No. 303-1015, Perkin Elmer Corporation, Norwalk, Conn.) with radii of 164 and 185 mm. The mirror was held in an aluminum mirror mount which consisted of an inner frame turning on a vertical axis, a second frame turning on a horizontal axis, and a third, stationary, frame. A micrometer (The L. S. Starrett Company, Athol, Mass.) mounted in the second frame was used to position the inner frame around the vertical axis. A set screw was used in the alignment of the second frame with respect to the stationary frame. This setup facilitated the focussing of the desired part of the image on the entrance slit of the monochromator and allowed a controlled horizontal scan across a light source. The Czerny-Turner grating monochromator (Model EU-700, Heath Company, Benton Harbor, Mich.) was provided with folding mirrors so that the entrance and exit beams were on a common optical axis.

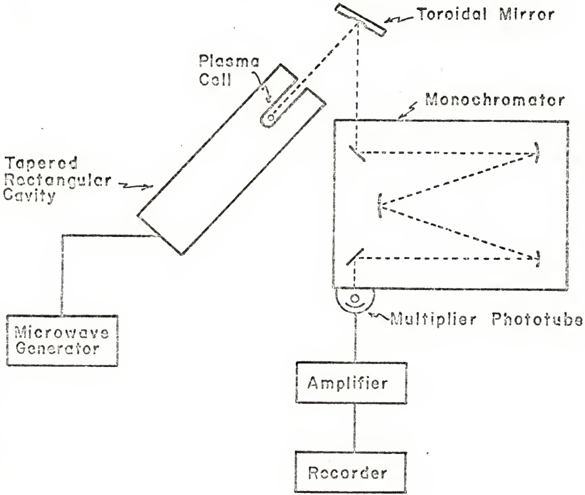

Fig. 4.-Schematic diagram of the optical and electrical system of the apparatus.

A wavelength control unit (Model EU-700-51, Heath Company) supplied pulses at nine controlled rates to the stepping motor which drove the scanning mechanism of the monochromator.

The plasma cell shown in Figure 5 was constructed of quartz tubing (Vitreosil standard transparent tubing, Thermal American Fused Quartz Company, Montville, N. J.). A piece of Teflon positioned the lower open end of the quartz on a copper rod and sealed the opening to keep air from entering the plasma. The copper rod was a part of the cell holder and was used to facilitate the initiation of the plasma discharge and also served to conduct heat away from the copper wire which anchored the lower end of the plasma. The 9 mm i.d. upper part of the cell reduced the amount of air which diffused back into the 2.3 mm i.d. discharge region.

A medical diathermy unit (PGM-10X1, The Raytheon Company, Waltham, Mass.) equipped with a reflected power meter (No. 725-3, Microwave Devices Inc., Farmington, Conn.) provided up to 120 watts at 2450 MHz. A tapered rectangular cavity (No. 7097-1001G1, The Raytheon Company) coupled the microwave power into the plasma.

Readout

The light emerging from the exit slit of the monochromator was detected by a potted 1P28 multiplier phototube. The photoanodic signal from the phototube was

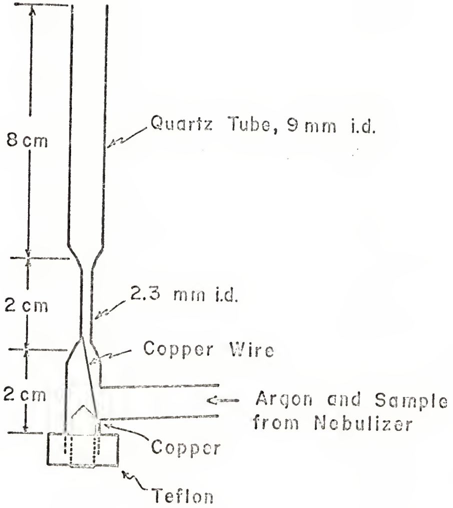

Fig. 5.-Quartz cell used to contain the plasma.

amplified by a DC photomultiplier microphotometer (No. 10-213, American Instrument Company, Silver Springs, Md.) or an electrometer (Model 610 BR, Keithley Instruments, Inc., Cleveland, Ohio) and was recorded on a one millivolt recorder (Servo/Riter Model PS01W, Texas Instruments, Inc., Houston, Texas).

Aerosol and gas

The argon was split into two streams after the two stage regulator which controlled the pressure. Each of the gas lines was equipped with a valve for controlling and a rotameter (No. 4-15-2, Ace Glass, Inc., Vineland, N. J.) for monitoring the gas flow. One of the streams of argon served to nebulize aqueous samples and carry the samples into the plasma. The second stream, which was mixed with the first stream before reaching the plasma cell, was used to reduce the concentration of water vapor in the plasma gas.

The system which produced the aerosol is shown schematically in Figure 6. The aspirator was similar to one used by Veillon and Margoshes [14], except that the capillary was made of stainless steel and the orifice was conical. The heated chamber was a 7.5 cm diameter glass tube wrapped with heating tape. A steady state temperature of about 130 C was reached in the chamber under the usual operating conditions. An aperture of about 1 mm i.d. vented

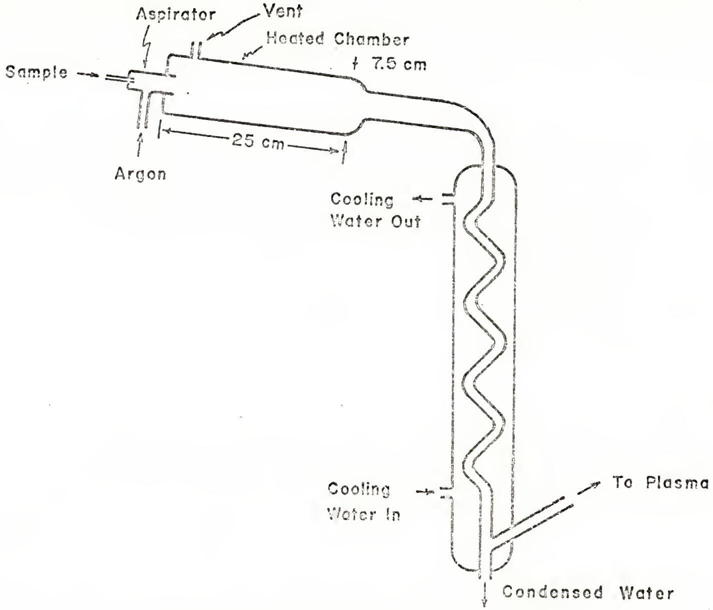

Fig. 6.-The dry aerosol producing system.

the chamber to the atmosphere in order to reduce back pressure in the system. After passing through the oven, the stream of argon, containing water vapor and salt particles, flowed through a condenser. The condenser, consisting of a fourteen turn, 5 cm diameter coil of 8 mm i.d. glass tubing inside a water jacket, served to remove most of the water vapor from the argon. A small pump (Model B-1, Eastern Industries, Hamden, Conn.) was used to circulate ice water through the condenser. An argon flow of 1.20 l/min reached the plasma cell. The stream which bypassed the aerosol system had a flow rate of 0.58 l/min, so the mixed argon was about 50 per cent dry argon and 50 per cent moistened argon. The solution uptake rate of the nebulizer was 1.1 ml/min.

Early cell designs

Before the design shown in Figure 5 was adopted, two other types of plasma cell were built and tested. The first cell tried was similar to that used by Kleinmann and Svoboda [28]. It consisted of a brass and Teflon chamber containing water-cooled copper blocks. Graphite holders mounted in the copper blocks held a graphite disk. Above the disk was a quartz chimney. Samples were introduced by applying a drop of solution to the graphite disk, and ohmic heat was applied. Low wattage was used at first in order to evaporate the solvent, and then about 200 watts were applied to vaporize the sample. An argon stream passed around the disk and served to carry the sample vapor and to support the plasma which was initiated after the solvent evaporation step. The plasma was contained by the quartz chimney which also kept air from mixing with the argon in the plasma region. The portion of the plasma which appeared in the lower part of the chimney was observed. Signals appeared as skewed Gaussian peaks similar to gas chromatographic peaks. Unfortunately, neither the peak height nor the peak area was constant for constant sample size. Consecutive measurements of samples of the same size varied by as much as a factor of two. Measurements for pure solvent gave no signals, so the irreproducibility of signals due to sample emission was not caused by a severe memory effect. Also, a large part of each peak appeared to be due to a change in the level of the plasma continuum caused by the sample vapors. Therefore, the results obtained for this cell were not good for either quantitative or qualitative analysis.

The second cell investigated consisted of an aluminum chamber containing a graphite cylinder held by two graphite bars mounted in water-cooled copper blocks. The argon stream which supported the discharge passed through the graphite cylinder into a quartz chimney at the top of the aluminum chamber. The aerosol system shown in Figure 6 was used with this cell design. It was intended that resistance heating of the graphite cylinder would vaporize the dry aerosol carried by the argon. The plasma which was initiated in the chimney would then serve to excite the vaporized sample. However, there were two serious drawbacks to this design. First, the plasma column in the chimney shifted constantly, and no method was found to anchor the discharge. Second, it was found that smaller signals and smaller signal-to-noise ratios were obtained when the graphite was heated than when it was not heated. Previously, Runnels and Gibson [27] had noted that preheating the argon stream resulted in reduced emission from argon atoms and metal atoms in the plasma. The reduced signal in the heated argon meant that the graphite cylinder cell system was not analytically useful.

The problem of a shifting plasma which was encountered during the study of the second cell also caused difficulties in early studies of the cell shown in Figure 5. Lengthening and shortening of the plasma was accompanied by movement of the plasma column around the walls of the cell. After several minor changes had been made in the cell design, it was found that a piece of copper wire, as shown in Figure 5, could anchor the lower part of the discharge. The upper portion of the discharge, which extended about 3 cm above the tapered rectangular cavity, still moved slightly, but the plasma column was nearly stationary along the wall of the cell in the region observed. Occasionally, the plasma would move, but, after a few seconds, it would return to its original position. Thus, this cell design proved adequate for measurements of plasma parameters and for analytical applications.

Initiation of the plasma

The plasma was relatively easy to initiate when dry argon passed through the cell. The procedure was as follows. The valve on the argon tank was opened, and the regulator pressure was adjusted to five pounds. Argon was allowed to flow for a few minutes to flush air from the system. Then the microwave generator was turned on to maximum power, and a spark was applied to the copper rod of the plasma cell with a Tesla coil. After the plasma was started, the generator was adjusted until the power meter read 100 watts forward power.

When the dry aerosol system was in operation, however, the plasma was difficult to initiate. The procedure for initiating the plasma when the aerosol system was to be used was as follows. First, the heating chamber of the aerosol system was turned on, and the pump which circulated ice water through the condenser was started. After a wait of about ten minutes, the argon was turned on and water was sprayed into the heated chamber. A period of five minutes was then allowed for air to be flushed from the system and for the oven temperature to approach its steady-state value. The microwave generator was then set at its maximum power output, and the line from the aerosol system was closed with a clamp so that only the dry argon stream passed through the cell. After the plasma had been initiated with a Tesla coil, the clamp of the tubing between the condenser and the plasma cell was opened, and the microwave power was adjusted so the forward power reading was 100 watts.

Adjustment of optics

The tapered rectangular cavity was positioned such that the slot was aligned with the optical axis (see Fig. 4). The quartz plasma cell was centered between the walls of the slot at the position along the slot at which the reflected microwave power was at a minimum. The microwave generator was adjusted to deliver 100 watts for all measurements. The generator was capable of providing 120 watts, but operation at power levels above 100 watts was found to result in overheating of the generator.

The toroidal mirror was placed on the optical axis of the monochromator at that position where the angle between the plasma cell and the monochromator was 40 degrees. The toroidal mirror and mount system described in Chapter II was positioned on its horizontal axis such that the image of the part of the plasma in the vertical center of the slot was focussed on the entrance slit of the monochromator. The slit width of the monochromator was set so the dial indicated 20 microns. Aperture disks were used to limit the height of the slits to 1 mm. These slit settings constituted a compromise because smaller slit widths and heights gave better resolving power, but reduced the amount of light reaching the phototube.

Monochromator calibration

A tungsten strip lamp calibrated by the National Bureau of Standards was used to obtain the calibration curves shown in Figure 7. The vertical scale is in relative units for all three curves shown. The curve of the lamp radiance versus wavelength was obtained by using the calibration values, tables of emissivities of tungsten, and Planck's Law to determine the temperature of the tungsten strip. Planck's Law is given by

$$B_\lambda(T) = (8\pi hc/\lambda^5)(\exp(hc/\lambda kT)-1)^{-1} \qquad (29)$$

where $B_\lambda(T)$ is the blackbody radiance in W cm^{-2} nm^{-1} ster^{-1}. Then the calculated temperature was used in the calculation of radiances for several wavelengths. The above procedure was used because the table of calibrated radiance values provided by the National Bureau of Standards did not have enough values for the construction of a smooth curve;

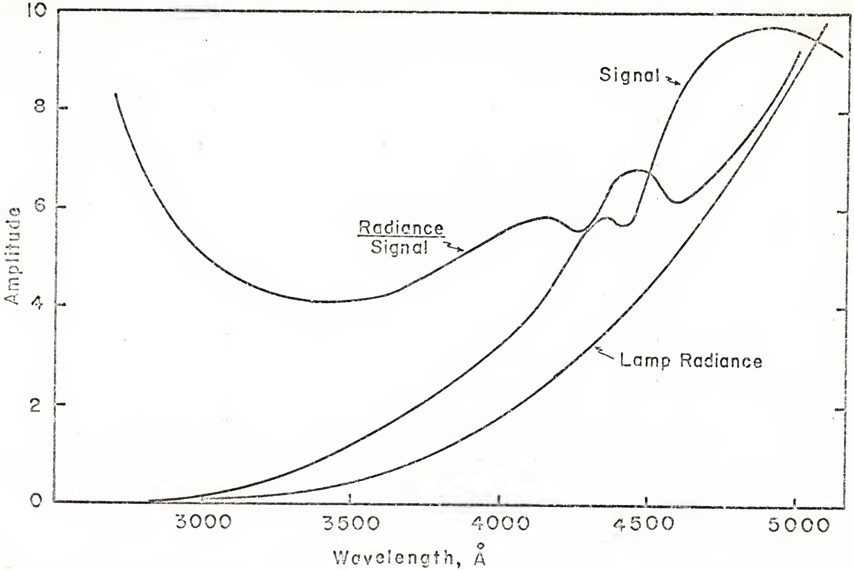

Fig. 7.-Relative calibration curves for the tungsten strip lamp and the optical system.

intermediate values were needed. The curve of the recorded signal versus wavelength exhibits an irregularity at about 4300 Å. This is a response peculiar to 1P28 phototubes.

In addition to the relative calibration curves shown in Figure 7, absolute calibration was effected at a few wavelengths. For example, at 4000 Å, a lamp radiance of 9.25×10^3 W cm^{-1} ster^{-1} resulted in a signal of 9.2×10^{-9} amp; the ratio of radiance to signal is then 1.01×10^{12} W amp^{-1} cm^{-2} nm^{-1} ster^{-1} at 4000 Å for a continuum or a line wider than the spectral bandwidth of the monochromator. For a line which is much narrower than the spectral bandwidth of the monochromator, the recorded signal results from the integrated radiance of the line. The equations relating radiance and signal for the continuum case and the narrow line case are as follows:

$$\mathrm{Signal})_{\mathrm{cont}} = C_\lambda B_\lambda s \tag{30a}$$

$$\mathrm{Signal})_{\mathrm{line}} = C_\lambda B_\ell \tag{30b}$$

where C_λ is a factor which takes into account the transmission of the monochromator optics and the phototube response at wavelength λ, as well as some monochromator and phototube parameters which do not change with wavelength, B_λ is the spectral radiance of a band or wide line and B_ℓ is the integrated radiance of a line. The factor C_λ has the units of amp cm^2 ster W^{-1} and has the same value in equations (30a) and (30b) if and only if the slit width of the monochromator is the same for both measurements. The spectral bandwidth of the monochromator is in units of nanometers and is represented by s.

Measurement of the spectral bandwidth

A value for the spectral bandwidth was necessary for the calibration of the system and for the determination of the electron density. The stepped wavelength drive of the monochromator made the measurement very easy. First, a light source was chosen which emitted a narrow line near the wavelength of interest. In this study, the slit width indicator was set at 20 microns before the system was calibrated and was kept at this value for all measurements, so adjustment of the slit width was not necessary. Next, the desired size of aperture disk was placed in front of the slit to set the slit height. After the mirror was adjusted so that the image of the source was centered on the entrance slit, a slow wavelength scan was made in the wavelength region of the line of interest. This was done in order to determine the wavelength indicated by the dial on the monochromator when the radiation falling on the exit slit was that of the emission line. Next, the wavelength was set at a value 2 Å below the line wavelength. The signal at this wavelength was monitored for 30 seconds, and then the wavelength was stepped by 0.1 Å and the signal was again monitored for half a minute. This was repeated until the wavelength was about 2 Å beyond the line wavelength. The average value of the signal for each of the 30 second measurements was then plotted versus wavelength. The result of such a plot for the 4671 Å xenon line is shown in Figure 8. The straight line portions of the curve wings are extrapolated down to the base line and upwards until the lines cross, so that a triangle is formed by the base line and the two extrapolated lines. The width of the triangle at its half height gives the spectral bandwidth. The line used to determine the spectral bandwidth should be fairly near the wavelength of interest because the spectral bandwidth is proportional to the reciprocal linear dispersion of the monochromator. The reciprocal linear dispersion is slightly dependent on wavelength, for example, conditions giving a spectral bandwidth of 0.61 Å at 4000 Å will give a spectral bandwidth of 0.65 Å at 3000 Å. The 4671 Å xenon line was employed to determine the spectral bandwidth used along with recorded signals from the 4861 Å hydrogen line in electron density determinations. At a wavelength of 4671 Å, the spectral bandwidth was 0.58 Å; this value differed from the spectral bandwidth at 4861 Å by about 0.005 Å.

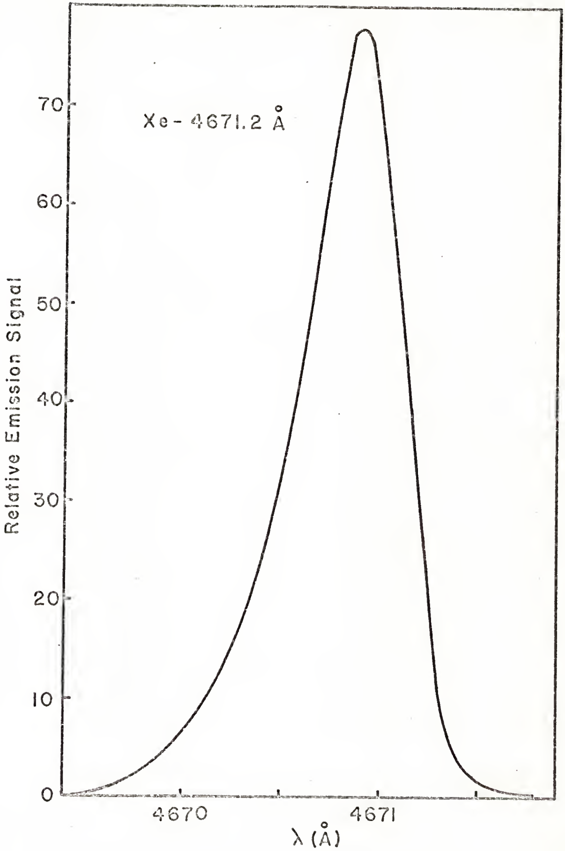

Fig. 8.-Slit function of the Heath monochromator.

Measurement of signals of argon lines

In order to make use of equations (7), (10) and (11) for estimation of plasma temperatures, it was necessary to obtain radiances of atomic lines in the plasma; the atomic argon lines emitted by the plasma were quite suitable for this purpose. The following procedure was employed to measure the signals of the lines. First the monochromator was set at the wavelength of an argon line, and the micrometer screw on the mirror mount was adjusted to the position resulting in the maximum photoanodic signal. Then, with the micrometer kept at the maximum signal setting, the wavelength of the monochromator was started scanning slowly from a wavelength 5 Å below the wavelength of the line. About 1 Å below the line wavelength, the wavelength control unit was set so that the wavelength could be stepped manually by 0.1 Å. The wavelength was stepped slowly until the maximum signal was obtained. The maximum signal was recorded for about one minute. Then the wavelength control unit was returned to a slow automatic scan setting. The signal was recorded from 5 Å below to 5 Å above the line of interest. The signal for the region from 3 to 5 Å to either side of the line served as the background reading. This process was repeated for several lines.

Signals were converted to radiances by applying equation (30b). Values of C_λ for each wavelength were obtained by applying equation (30a) to the calibrated radiances and observed signals of the tungsten strip lamp. The spectral bandwidth was obtained by the method described in the next section.

Measurement of signals of lines of the 0,0 band of the $^2\Pi \rightarrow {}^2\Sigma$ OH system

The process used for the measurement of the signals of the lines in the 0,0 band of the $^2\Pi \rightarrow {}^2\Sigma$ system of the OH molecule was the same as that used for argon lines. However, the wavelengths of the lines in the OH band system are very close together so that many of the lines overlap. Only a few lines were free from overlap when the monochromator was used in the first order. Use of the monochromator in the second order doubled the resolving power and increased the number of lines for which overlap was negligible. Fortunately, the radiance of the 0,0 band was high enough so that even the small proportion of the light thrown into the second order by the 2500 Å blaze grating was sufficient for accurate measurements. The second order light level was about thirty-fold less than the first order level.

Measurement of the profile of the hydrogen beta line

Measurements of the line profile of the hydrogen beta line were necessary for electron density determinations. Initially this measurement of the line profile was done in a manner similar to that used in the measurement of the spectral bandwidth. Signals were recorded every 0.1 Å over the width of the hydrogen line. This method proved to be very time consuming because the hydrogen line was as much as 16 Å wide. Also, the chances of the plasma conditions changing slightly during the long period required for the measurement were very high. Therefore, the following method was used in the latter part of this investigation. The wavelength control unit was set for a scan of 0.05 Å/sec. The scan was started at a wavelength about 12 Å below the wavelength of the line center. As the scan proceeded, a card was used to interrupt the light beam at 1 Å intervals. This resulted in very narrow negative spikes in the recorded signal. These spikes served as wavelength reference points for the interpretation of the data and also were a convenient check on the constancy of the scan speed. The effect of the spikes on the recorded profiles was negligible.

Measurement of the axial signal profile of the plasma

Axial signal profiles of argon lines and OH lines were obtained by the following technique. First, the wavelength setting of the monochromator was adjusted to the wavelength of the line of interest. Then the micrometer screw on the mirror mount was adjusted until the edge of the plasma image fell on the entrance slit of the monochromator.

This was the point at which the observed signal changed from the dark current value of the phototube to a slightly larger value. Then the position of the micrometer was noted on the recorder chart paper near the recording of the signal. Next, the position of the micrometer screw was changed by one or two units on its vernier scale, and the signal was again recorded. This process was repeated until the mirror had been moved enough so that the entire image of the plasma had traversed the slit. The same procedure was used to obtain the plasma continuum profile about 5 Å away from the line measured. An axial signal profile was the result when the continuum profile was subtracted from the profile at the wavelength of the line.

Analytical curves

Values of the photoanodic signal due to emission were obtained as follows. After positioning of optical components and adjustment of electrical components, the sample solution was introduced into the dry aerosol system. A period of one minute was allowed for the aerosol to reach the plasma cell. The amplifier range was set such that the photoanodic signal resulted in a recorder readout that was on scale. After this reading was taken, pure solvent was introduced, and a background reading was taken at the same instrument setting. The emission signal was obtained by subtracting the background signal from the sample solution signal. Photoanodic signal readings were obtained over a wide range of solution concentrations, and plots of signal versus sample concentration were made from the resulting data.

Calibration of the micrometer screw

During the course of this investigation, it became necessary to know the distance in the plasma which corresponded to the unit markings on the micrometer screw of the mirror mount. These measurements were made in the following manner. The internal and external diameters of the narrow central part of the quartz plasma cell were measured. Then the cell was positioned in the tapered rectangular cavity, but the plasma was not initiated. Instead, a mercury pen lamp was positioned directly above and in contact with the open upper end of the quartz cell. The quartz then acted as a light pipe. The pen lamp supplied enough light so that the image of the illuminated cell, which was focussed on the monochromator entrance slit, was visible to the eye. The monochromator was set to the mercury 2536.5 Å line. Then the technique employed to obtain axial signal profiles was used on the image of the cell. This "cell profile" and the measured dimensions of the cell were used to correlate the micrometer readings with distance.

CHAPTER IV

RESULTS AND DISCUSSION

Appearance and spectra of the plasma

Under the operating conditions used during most of this investigation, the predominant color of the plasma was pink. As the amount of dry argon mixed with the argon coming from the dry aerosol system was decreased, the diameter and the length of the plasma decreased. The decrease in diameter was accompanied by a shift in predominant color from pink to blue.

The usual conditions of 0.58 l/min dry argon, 0.62 l/min wet argon and a solution uptake rate of 1.1 ml/min produced a plasma which varied in length from 6 to 7 cm and was about 0.3 mm in diameter. The plasma column tended to follow the contour of the quartz wall on one side of the cell. Without the copper wire in the cell, both ends of the plasma wandered constantly, and the length changed frequently. With the copper wire in the cell, only the upper end of the plasma was free to move. Copper emission was not observed in the spectrum.

A background spectrum of the plasma is shown in Figures 9 and 10. A ten times more sensitive amplifier

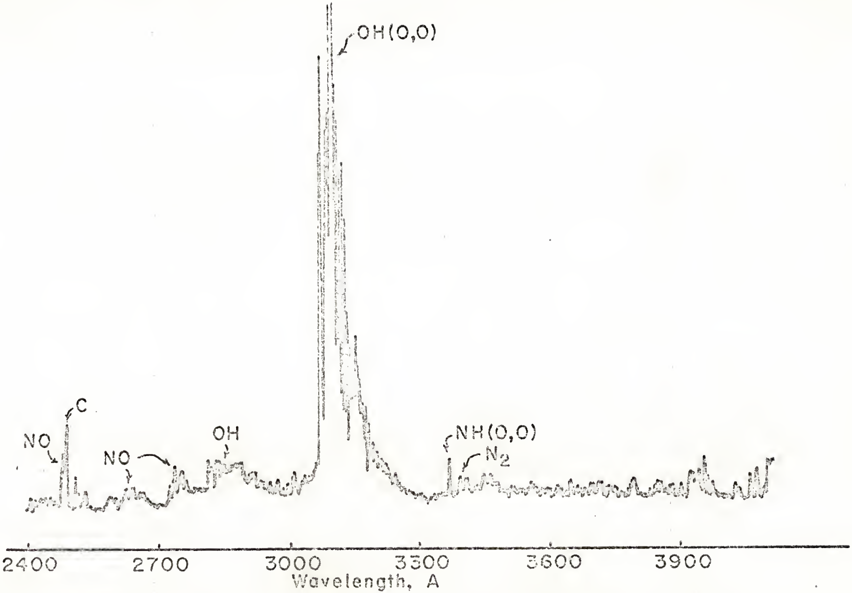

Fig. 9.-The background spectrum of the plasma from 2400 to 4100 Å.

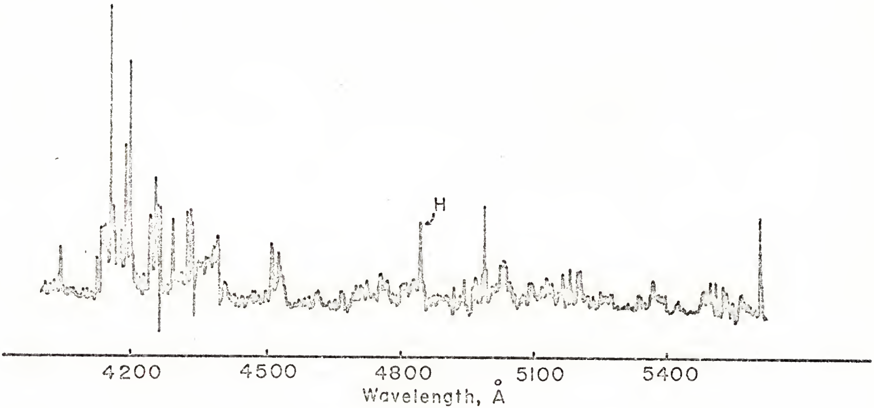

Fig. 10.-The background spectrum of the plasma from 4100 to 5600 Å.

scale was used for the part of the spectrum shown in Figure 10 than for the Figure 9 part. Some of the more prominent features have been labeled on the spectrum. With the exception of a single hydrogen line, all the lines which appear in Figure 10 are argon atomic lines. Use of a more sensitive amplifier scale would make apparent several more argon lines as well as two more hydrogen lines. The spectral region between 3400 and 4100 Å contains additional N_2 bands as well as a few argon atomic lines. The spectral region above 5500 Å has several strong argon lines which contribute to the pink color. The response of the 1P28 phototube is poor in this region, so a spectrum was not recorded.

Shown in Figure 11 is a recorder trace of a segment of the 0,0 band of the $^2\Pi \rightarrow {}^2\Sigma$ OH electronic band system. This trace was made in the first order of the grating, so the resolution is not as good as that used for rotational temperature determinations.

Temperature measurements in the plasma

The values of wavelengths, energies, and transition probabilities for the argon lines used in temperature determinations are given in Table 1. These values are the ones given by Malone and Corcoran [44]. The right hand column in the table has values for $\log(c'\lambda_{qp}/g_q A_{qp})$ where c' is a function of wavelength which is obtained from the relative curve of radiance/signal given in Figure 7. A c'

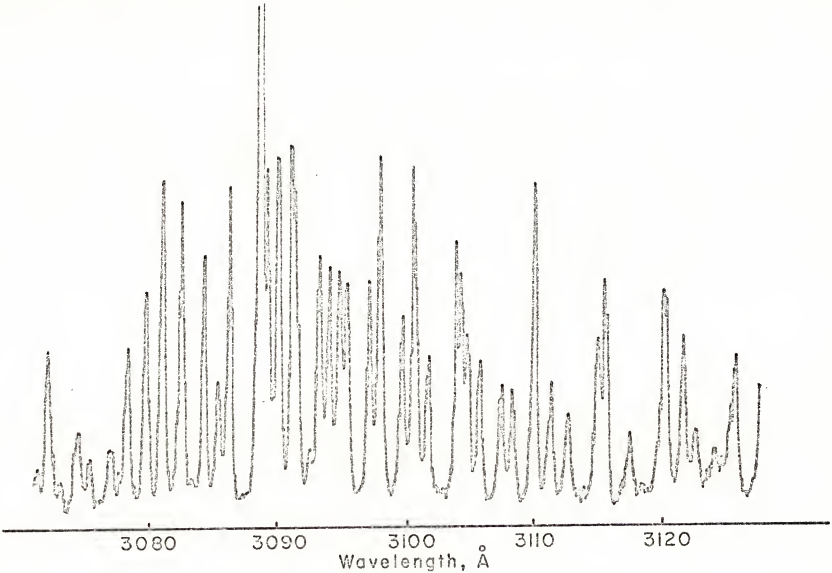

Fig. 11.-Spectrum of part of the OH 0,0 band system.

TABLE 1

WAVELENGTHS, ENERGIES AND TRANSITION PROBABILITIES[a] FOR ARGON LINES USED IN TEMPERATURE DETERMINATIONS

λ_{qp}, Å	E_q, cm^{-1}	$A_{qp} \times 10^{-5}$, sec^{-1}[a]	$\log(\frac{\lambda_{qp}}{g_q A_{qp}}) + 5$	$\log(\frac{c'\lambda_{qp}}{g_q A_{qp}}) + 5$[b]
3606.5	121470.3	6.96	2.715	2.604
4158.6	117183.7	12.42	1.820	1.836
4164.2	117151.4	2.28	2.784	2.800
4181.9	118459.7	4.87	2.457	2.472
4198.3	117563.0	24.22	2.239	2.251
4200.7	116942.8	8.01	1.875	1.887
4251.2	116660.1	0.89	3.202	3.202
4259.4	118871.0	36.65	2.065	2.066
4266.3	117183.7	2.65	2.508	2.510
4272.2	117151.4	6.88	2.316	2.319
4300.1	116999.4	3.18	2.435	2.442
4333.6	118469.1	5.06	2.234	2.256
4335.3	118459.7	3.08	2.673	2.696
4345.2	118407.5	2.73	2.724	2.754
4510.7	117563.0	10.12	2.648	2.731

[a] Transition probabilities are those determined by Malone and Corcoran [44].

[b] The factor c' corrects for the variation of response of the instrumental system with wavelength. A value of one was arbitrarily chosen for 4251.2 Å.

value of one was arbitrarily chosen for the 4251.2 Å argon line. The relative correction, c', was used for the logarithmic plot method of temperature determination. In Figure 12, logarithmic plots of argon lines for two experimental conditions are given. The lower plot is obtained for the case where no water is aspirated into the dry aerosol system. For the other plot, the solution uptake rate was 1.1 ml/min, and the argon mixture was about 50 per cent dry argon.

The energies, wavelengths, and transition probabilities for the OH lines used in temperature determinations are given in Table 2. The values are those given by Dieke and Crosswhite [37]. The right hand column in Table 2 lists values of $\log(c'A'\nu')$, where c' is a factor which includes the response/signal correction relative to the $P_2(14)$ line, and a correction for an unresolved doublet line for each line in the Q_1, Q_2 and P_2 branches. The term ν' is the ratio of the frequency of the particular line to that of the $P_2(14)$ line.

Two OH logarithmic plots are shown in Figure 13. The lower plot is that for the case of no aspiration of water. The small amount of water necessary for OH radicals in the argon came from impurities in the tank or from moisture in the gas flow system. The concentration was small enough, however, that many of the lines could not be

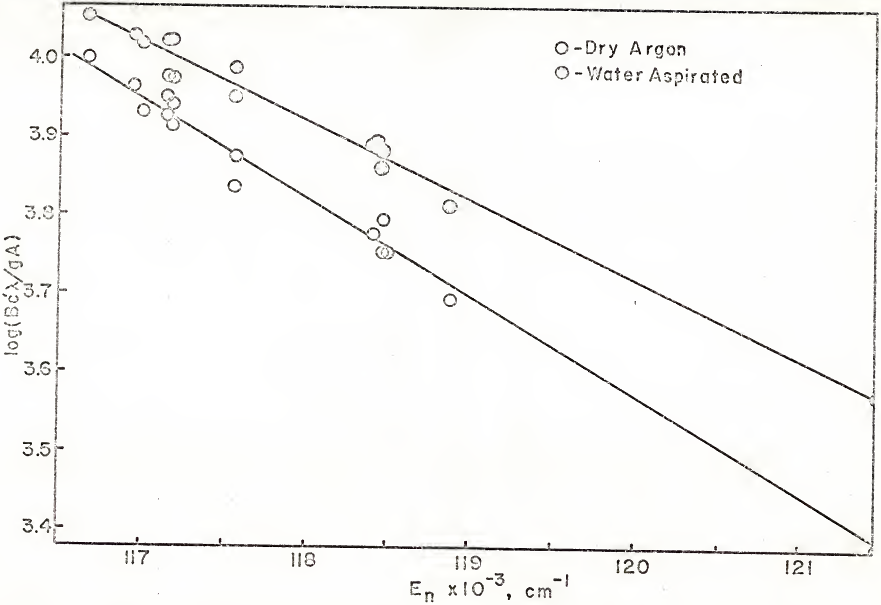

Fig. 12.-Logarithmic plots for argon lines for two plasma conditions.

TABLE 2

WAVELENGTHS[a], ENERGIES AND TRANSITION PROBABILITIES FOR THE ROTATIONAL LINES OF THE ELECTRONIC BAND SYSTEM OF OH USED IN TEMPERATURE DETERMINATIONS

Line	Wavelength, Å	E_k, cm^{-1}	log(A')[b]	log(c'A'ν')[c]
$R_2(4)$	3074.37	32947.05	1.143	1.131
$R_2(7)$	3069.18	33650.38	1.433	1.419
$R_2(14)$	3071.15	36393.24	1.765	1.751
$Q_1(6)$	3087.34	33150.14	1.735	1.742
$Q_1(9)$	3095.34	33951.80	1.907	1.905
$Q_1(13)$	3110.22	35462.01	2.059	2.053
$Q_1(14)$	3114.77	35914.82	2.088	2.083
$Q_1(19)$	3143.01	38597.79	2.206	2.204
$Q_2(7)$	3094.62	33383.26	1.735	1.737
$Q_2(8)$	3096.83	33650.38	1.800	1.797
$Q_2(12)$	3109.33	35035.86	1.988	1.980
$Q_2(13)$	3113.36	35459.02	2.023	2.018
$Q_2(16)$	3127.68	36902.90	2.113	2.107
$Q_2(17)$	3133.22	37440.15	2.137	2.133
$P_1(5)$	3101.23	32779.49	1.414	1.404
$P_1(6)$	3106.54	32948.31	1.480	1.472
$P_1(9)$	3123.95	33652.29	1.628	1.622
$P_1(12)$	3143.80	34645.53	1.733	1.730
$P_1(13)$	3151.00	35038.61	1.762	1.760
$P_1(14)$	3153.51	35462.01	1.788	1.787
$P_2(4)$	3103.27	32643.45	1.136	1.266
$P_2(5)$	3107.55	32778.49	1.264	1.342
$P_2(7)$	3117.19	33148.73	1.436	1.463

Table 2 Cont'd.

Line	Wavelength, Å	E_k, cm^{-1}	log(A')^b	log(c'A'ν')^c
$P_2(10)$	3134.34	33949.67	1.603	1.604
$P_2(11)$	3140.73	34280.64	1.645	1.645
$P_2(14)$	3161.89	35459.02	1.747	1.747

---

[a] Values for the wavelengths and for the energies of the upper states are those listed by Dieke and Crosswhite [37].

[b] To obtain the A' values, line strengths from Dieke and Crosswhite [37] are multiplied by (')^3, where ' is the ratio of the frequency of the particular line to that of the $P_2(14)$ line.

[c] The factor c' corrects for the variation of response of the system with wavelength and also, for the Q_1, Q_2, and P_2 branches, corrects for an unresolved doublet line.

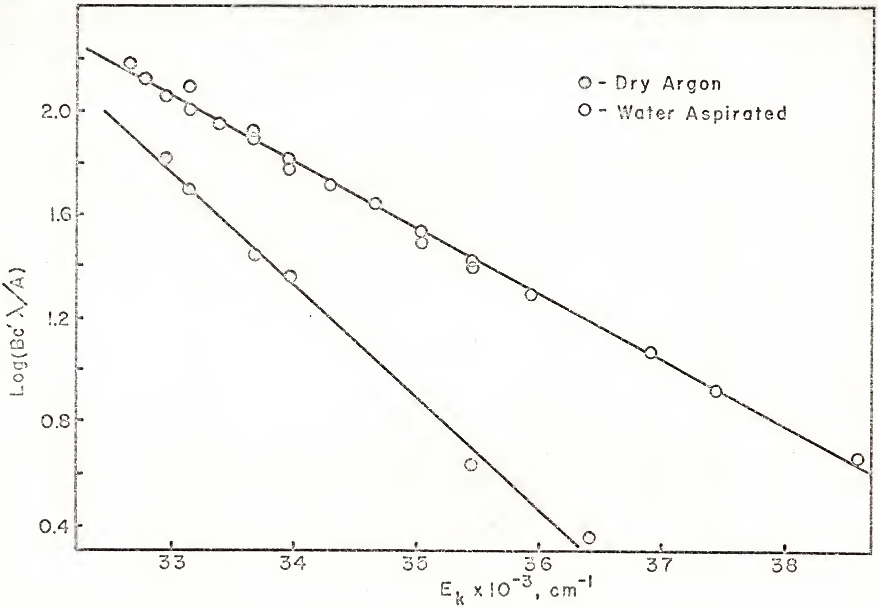

Fig. 13.-Logarithmic plots for OH lines for two plasma conditions.

measured accurately in the second order because of low signals. Signals were especially small for the higher lines of the branches. Because of the small signals, only six lines were used. The second plot in Figure 13 was for the case where the solution uptake rate is 1.1 ml/min, and dry argon comprised one half of the total flow.

From the slopes of the plots in Figure 12, excitation temperatures of 4980 K for dry argon and 6280 K for "wet" argon are obtained. The logarithmic plots in Figure 13 for the lines from the OH electronic bands result in rotational temperatures of 1440 K for dry argon and 2440 K for wet argon.

Axial signal profiles were obtained for three argon lines and three OH lines. Equations (28a) and (28b) and Barr's weighting factors [42] were used to transform the axial profiles into radial profiles. Figures 14, 15 and 16 each show the observed axial profile and transformed radial profile of an argon line. In each of the argon profiles, the right side of each figure corresponds to the side of the plasma which was closest to the quartz cell wall. Figure 17 shows the axial radiance profiles of three OH lines. The resulting radial profiles are given in Figure 18. For the CH lines, the left sides of Figures 17 and 18 correspond to the side of the plasma nearest the cell wall. The profiles for OH and argon were measured and drawn in

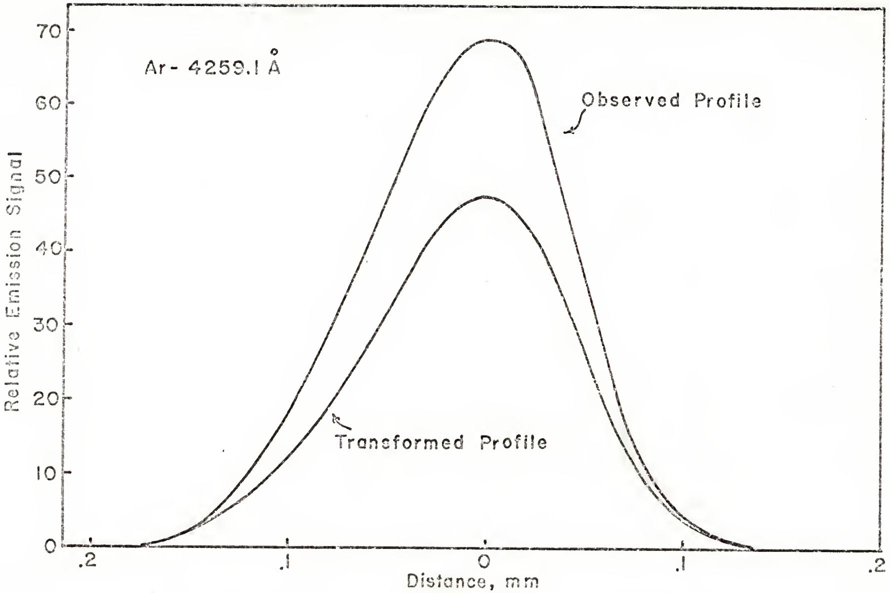

Fig. 14.-Observed and transformed plasma signal profiles for the 4259.1 Å line of argon.

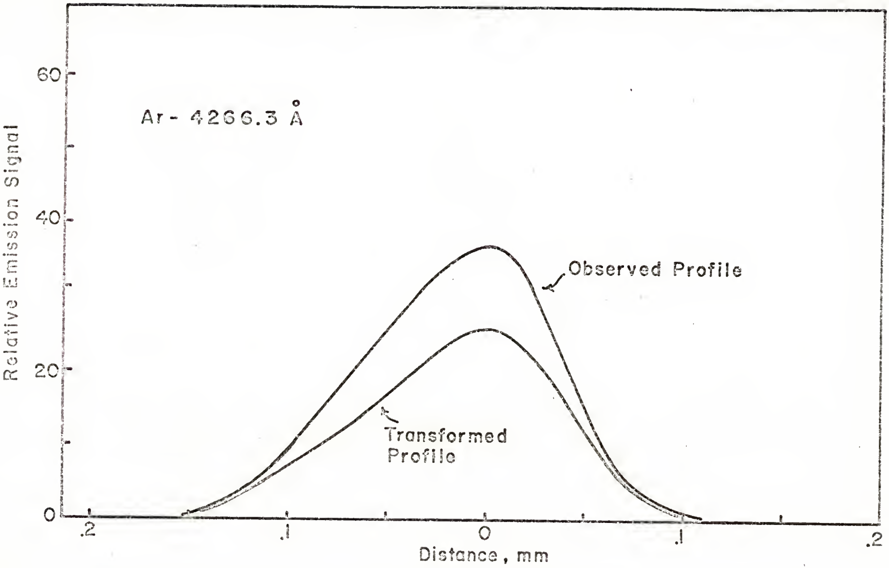

Fig. 15.-Observed and transformed plasma signal profiles for the 4266.3 Å line of argon.

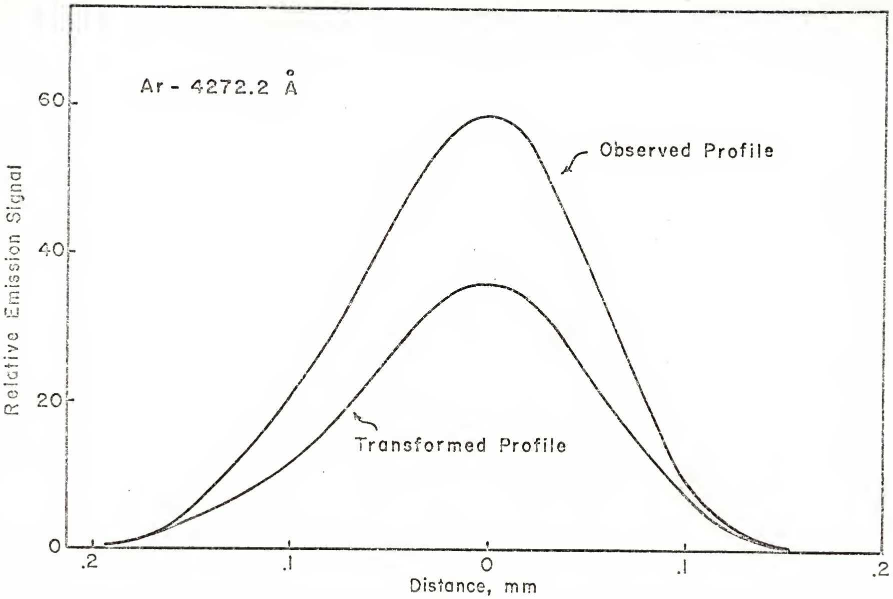

Fig. 16.-Observed and transformed plasma signal profiles for the 4272.2 Å line of argon.

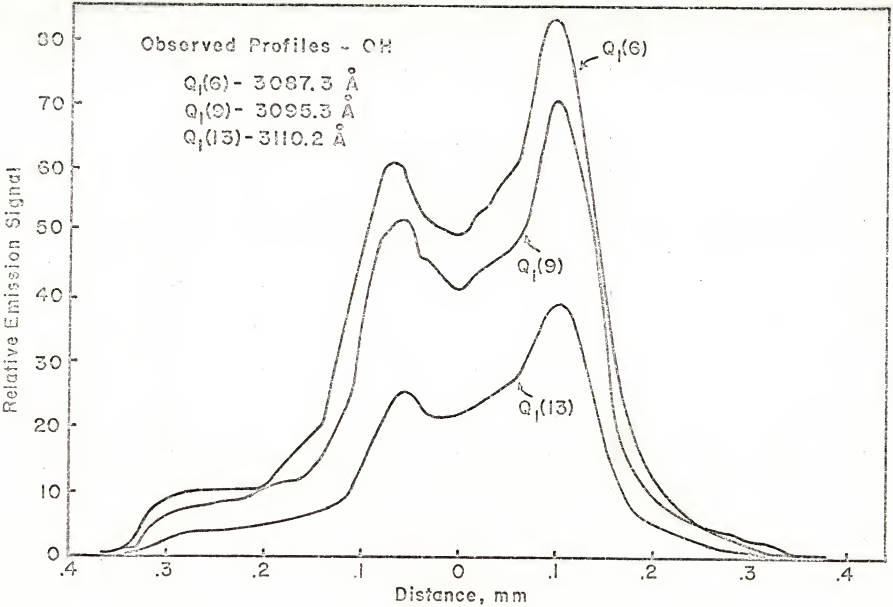

Fig. 17.-Observed signal profiles of the plasma for the $Q_1(6)$, $Q_1(9)$ and $Q_1(13)$ lines of the 0,0 OH band.

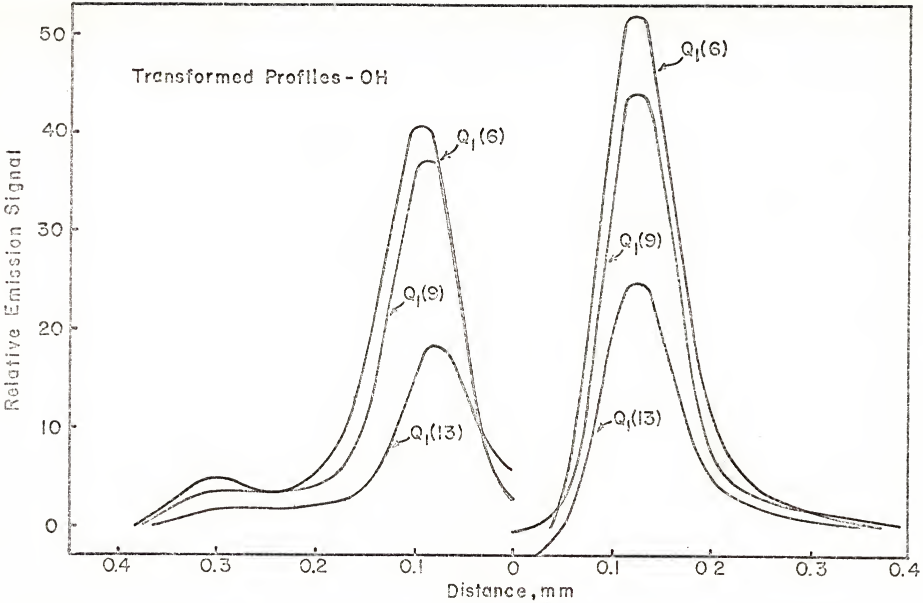

Fig. 18.-Transformed signal profiles of the plasma for the $Q_1(6)$, $Q_1(9)$ and $Q_1(13)$ lines of the 0,0 OH band.

the same direction but different cells of the same design were used. In the most stable plasma configuration for the cell used during the argon measurements, the plasma was near the left side of the cell, while in the cell used during the OH measurements, the plasma was on the right side of the cell.

A plot of the logarithm of the radiance versus temperature for the 4259.4 Å line of argon is given in Figure 19. Values from Table 1 were used in equation (7) to obtain the plot. A path length of 0.03 cm was obtained from the argon radial profiles. Calculations by Goldman [45] show that the partition function, Q, for argon is nearly equal to one up to a temperature of 10,000 K (at 10,000 K, Q is equal to 1.0001). The observed and the transformed signal profiles from Figure 14 and the plot in Figure 19 were used to obtain the temperature profiles shown in Figure 20. The left sides of the signal profiles were used because of errors in the right sides of the profiles due to the proximity of the wall to the plasma. Observations of the plasma indicated that its cross section was probably shaped like a circle which was slightly flattened on one side. This resulted in errors in the radial profile obtained from the Abel transformation of the axial profile. A maximum temperature of 8520 K was obtained from the axial profile, while the radial signal profile gave a maximum temperature of 9010 K.

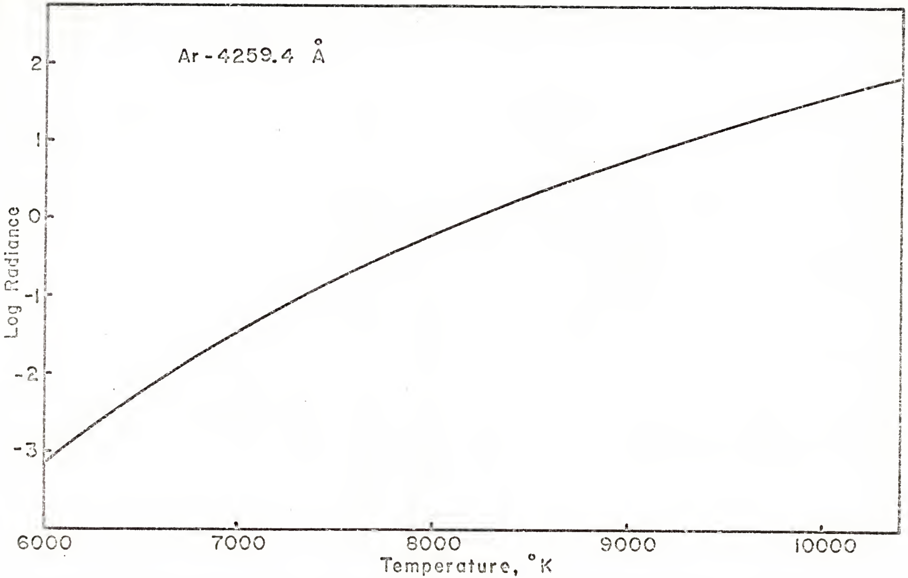

Fig. 19.--Relationship between the radiance of the argon 4259.4 Å line and the temperature.

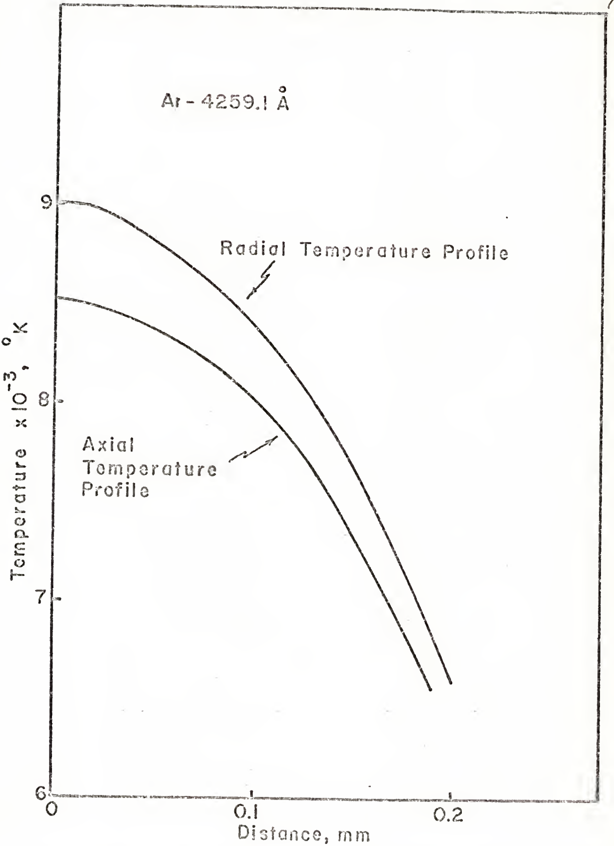

Fig. 20.-Temperature profiles in the plasma for two plasma conditions.

Electron density measurements

The method described in Chapter III was used to obtain the hydrogen line profile shown in Figure 21. The relationship

$$\Delta\lambda_T = (\Delta\lambda^2 + s^2 + \Delta\lambda_D{}^2)^{1/2} \quad , \qquad (31)$$

where $\Delta\lambda_T$ is the total half width and $\Delta\lambda_D$ is the Doppler half width, was used to calculate the Stark half width, $\Delta\lambda$, from the measured $\Delta\lambda_T$. The plot in Figure 2 was used to find the electron density which corresponded to the value of $\Delta\lambda$. Hydrogen line profiles taken at several positions in the plasma were used to obtain the electron density profile shown in Figure 22. The maximum electron density indicated by the profile is 2.6×10^{15} electrons cm^{-3}.

An attempt was made to perform the Abel transform on the hydrogen line profiles. This required that axial signals be measured at each of several wavelengths over the hydrogen line. However, the matter became complicated because both the temperature and the electron density decreased as distance from the center of the plasma increased. Thus, the area of the hydrogen line increased with temperature while the width of the line increased with electron density. The result was that, in going from the edge of the plasma to its center, the height of the hydrogen line first increased, then passed through a maximum

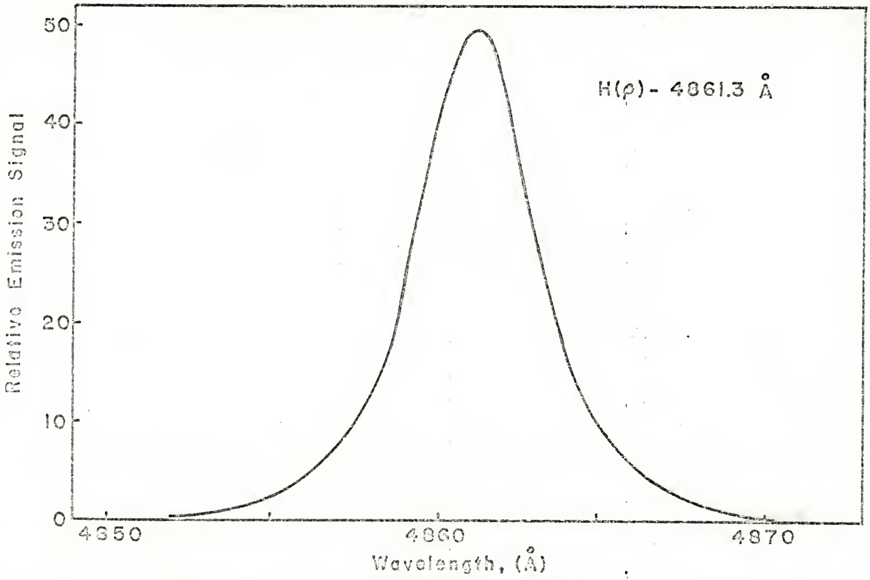

Fig. 21.-Observed profile of the hydrogen beta line.

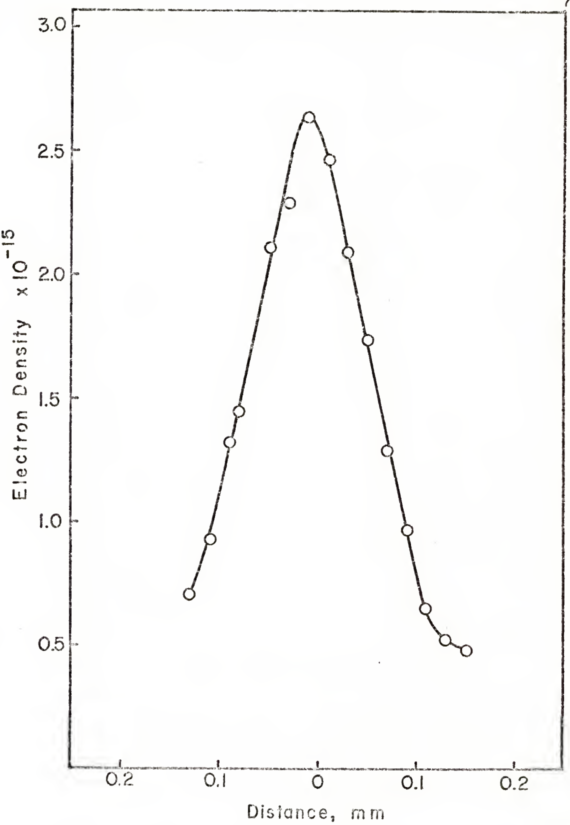

Fig. 22.-Variation of electron density with position in the plasma.

and decreased again. Radial transforms are then subject to large errors near the line center if even small errors are made in the measured values. The attempted transform of the hydrogen profile indicated a maximum electron density of 6 x 10^{15} electrons cm^{-3} at the center of the plasma. However, very little confidence may be placed in this value.

Summary of plasma properties

Table 3 gives diameters, temperatures and electron densities for the plasma under two sets of conditions. One set of data is given for the case where no water is aspirated. The second set is for the case where the solution uptake rate is 1.1 ml/min. In each case, there is a large difference between the rotational temperature and the excitation temperature. As noted in Table 3, the rotational temperature of 2440 K given is that obtained from the axial profile at a point 0.08 mm from the center of the plasma (maximum OH signals and OH rotational temperatures were obtained at this distance), for the second case. At this point in the plasma (0.08 mm), the excitation temperature obtained from the axial radiance of argon is about 8200 K while the radial radiance gives a temperature of about 8600 K. This large temperature difference between the rotational temperature and the excitation temperature shows that local thermodynamic equilibrium does not exist in the

TABLE 3

PROPERTIES OF THE MICROWAVE DISCHARGE THROUGH ARGON

	Without Aspiration	Aspiration of 1.1 ml/min of H_2O
Diameter radiating Argon lines	0.8 mm	0.3 mm
Diameter radiating OH bands	1.2 mm	0.6 mm
Temperature from Argon line logarithmic plot	4980 K	6280 K
Temperature* from a logarithmic plot of OH rotational lines from the 0,0 vibrational band	1440 K	2440 K
Temperature from the axial radiance of the Argon 4259.4 Å line	7990 K	8520 K
Temperature from the radial profile of the Argon 4259.4 Å line	8200 K	9010 K
Maximum electron density	3.0×10^{14}	2.6×10^{15}

*For the case without aspiration, the maximum temperature from OH lines is obtained 0.25 mm from the center of the discharge. For the other case, the distance is 0.08 mm from the center.

plasma. There is also a fairly large difference between temperatures obtained by the absolute radiance method.

If radial signals rather than axial signals had been used to make the plots, better temperature values would have resulted. Temperatures calculated from axial signals are averages of temperatures in several zones of the plasma, while temperatures calculated from radial signals are temperatures of single zones. However, the time involved in measuring the axial profiles would have been prohibitively large. About forty minutes was required for the measurement of a profile of one line. The possibility of a slight change in the plasma conditions, or of the microwave generator's circuit breaker opening, was very large after a running period of more than four hours. The radial profiles of the three lines which were investigated give a logarithmic plot temperature of about 6800 K at the plasma center. Three lines, however, are not sufficient for an accurate temperature determination.

Several explanations are possible for the discrepancy between the logarithmic plot temperatures and the absolute radiance temperatures. Possibly, errors in the transition probabilities used, in the path length chosen, or the radiance calibration of the system account for the difference. All of these sources of errors affect the temperatures calculated from absolute radiances to a greater degree than the temperatures derived from the logarithmic plot method. It is also possible that the difference in temperatures obtained from the two methods results from the deviation from equilibrium in the plasma.

The transformed profiles shown in Figure 18 for the OH lines indicate that the concentration of OH in the center of the plasma approached zero. On one side of the profiles, the transform gave negative radiances. This was due to a small error in picking the center of the plasma. Perhaps the deviation from a cylindrical plasma shape also contributed. The logarithmic plot method for the three transformed OH lines indicates a temperature about 200 K higher than that obtained from the axial profiles by the same method. Of course, the use of only three lines does not lend much certainty to either the plot of axial signals or the plot of radial signals.

A qualitative examination of equilibrium constants, ionization potentials, and dissociation energies indicates that the OH molecule dissociates into monatomic oxygen and hydrogen under the conditions in the plasma center. The large degree of dissociation explains the low level of OH emission from the plasma. The oxygen and hydrogen resulting from the dissociation probably comprise the major part of the ionized species in the plasma because the ionization potentials for these two elements are lower than that of argon by more than 2 ev. The fact that the electron density in the dry argon plasma is smaller than that in the wet argon plasma indicates that decomposition products of water are the major ionized species. Also, an examination of Figures 18 and 22 shows that the electron density begins to rise sharply at the same distance from the plasma center that the signal due to OH reaches its maximum before dropping sharply as the distance from the center of the plasma decreases.

Analytical results

Analytical curves of five elements were obtained by atomic emission. Analytical curves for indium and gallium are shown in Figure 23. Figure 24 has analytical curves for zinc and mercury and two curves for cadmium. For each element, the peak-to-peak noise on the signal was recorded at a wavelength about 2 Å beyond the wavelength of the line used. The values of the noise and the slopes of the analytical curves were used to extrapolate limits of detection. The wavelengths used, the lowest concentrations measured, the analytical curve slopes obtained, the limits of detection estimated, and the percent standard deviations are listed in Table 4. Atomic emission of boron, calcium, strontium and lead was also observed, but analytical curves were not obtained. For all of the elements except boron, emission from a position outside of the visible part of the plasma gave the best signal to noise ratios.

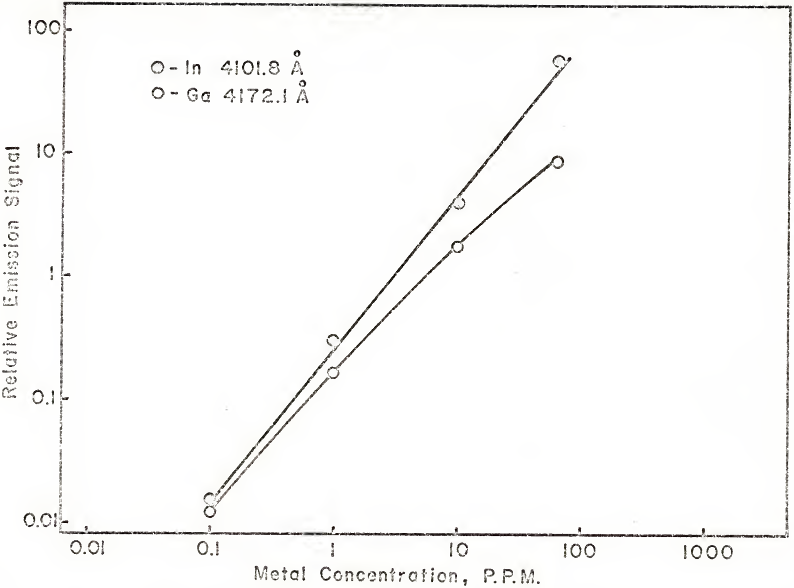

Fig. 23.-Analytical curves for indium and gallium.

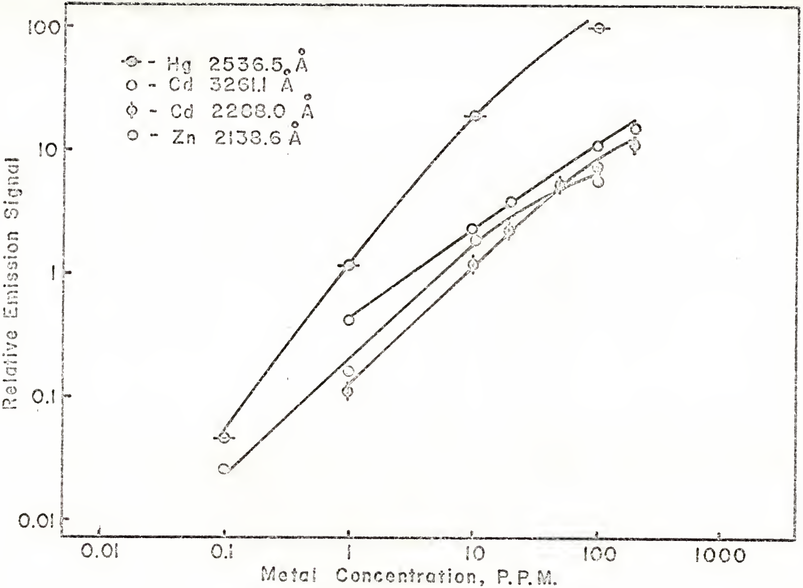

Fig. 24.-Analytical curves for mercury, cadmium and zinc.

TABLE 4

WAVELENGTHS, DETECTION LIMITS AND STANDARD DEVIATIONS FOR FIVE ELEMENTS

Element	Wavelength, Å	Lowest Concentration on Working Curve, ppm	Slope of Working Curve	Estimated[a] Limit of Detection, ppm	% Standard Deviation[b] at 1 ppm
Cadmium	2288.0	1	1.02	0.03	4.8 (5)
Cadmium	3261.1	1	0.83	0.07	9.2 (6)
Galium	4172.1	0.1	1.03	0.07	3.0 (5)
Indium	4101.8	0.1	1.12	0.07	6.4 (4)
Mercury	2536.5	0.1	1.31	0.03	4.0 (5)
Zinc	2138.6	0.1	1.04	0.03	4.8 (4)

[a] The noise level used in calculating the estimated limit of detection was that measured on the background, that is, water aspirated, about 2 Å from the wavelength of the analytical line.

[b] The numbers in parentheses are the numbers of measurements made.

An axial signal profile of the plasma at 2138.6 Å for the case where 2 ppm zinc solution was being aspirated is shown in Figure 25. Also shown in the figure is the background axial signal profile for 2141 Å for the case where water was aspirated. A position about 0.3 mm to the right of the point of maximum emission signal gave the best analytical results for all elements tried except boron, even though the net emission signals due to the elements were greatest in the center of the plasma.

Boron, however, gave the best results in the center of the plasma. The limit of detection for boron was about 0.5 ppm in the center of the plasma, while at the position used for the other elements, 10 ppm of boron could not be detected. Apparently the high energy available in the center of the plasma is necessary to decompose the oxides of boron.

Listed in Table 5 are the properties of the part of the discharge used for analytical measurements. Emission signals due to atoms and ions of calcium and strontium were used in equation (15) to obtain temperatures. These ion temperatures compare favorably with the temperature gotten from the logarithmic plot for argon lines. Again, the temperature determined from the absolute axial radiance of the 4259.4 Å argon line differs from the other values by a fairly wide margin.

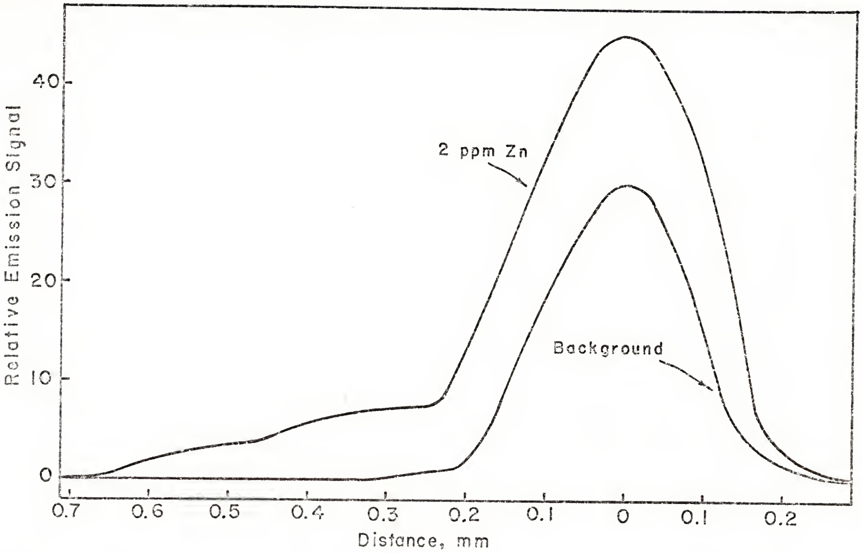

Fig. 25.-Change of signal with distance from the center of the plasma for the plasma background and for zinc emission.

TABLE 5

PROPERTIES OF THE PART OF THE DISCHARGE USED FOR THE ANALYTICAL CURVES

Electron density	1.8×10^{15} cm^{-3}
Temperature determined from the ratio of radiances of the 4077.7 Å Sr(II) line and the 4607.3 Å Sr(I) line	5050 K
Temperature determined from the ratio of radiances of the 3968.5 Å Ca(II) line and the 4226.7 Å Ca(I) line	4980 K
Temperature determined from a logarithmic plot for Argon	4920 K
Temperature determined from the axial radiance of the 4259.4 Å Argon line	6560 K

One serious difficulty was encountered during the analytical investigations. It was found that the quartz cell suffered from a memory effect. Some of the metal atoms which collided with the hot quartz walls apparently became trapped in surface irregularities of the quartz. A long time was required for the emission signals of the metal to fall to a negligible value after sample aspiration was halted.

Because of the memory problem, future investigations of the plasma will require a better cell design. A cross-shaped cell might solve the problem. The plasma would be contained in the vertical part of the cross while the plasma would be observed through a window on the end of the horizontal part. A stop placed inside the horizontal tube just before the window should reduce the amount of light piped by the quartz which reaches the monochromator.

Studies of the plasma for microwave power greater than 100 W should also be done. With greater power available, it should be possible to reduce the proportion of dry argon without sacrificing plasma stability.

The plasma studied here shows promise for analytical applications. Further study is necessary, however, before this plasma can become a practical analytical tool.

BIBLIOGRAPHY

1. A. Gatterer, Spectrochim. Acta, 3, 214(1948).

2. R. Mavrodineanu and H. Boiteux, "L'Analyse Spectrale Quantitative Par La Flamme," Masson et Cie, Paris, 1954.

3. G. D. Cristescu and R. Grigorovici, Bull. Soc. Phys. Roumaine, 42, 3(1941).

4. E. Bădărău, M. Giurgea, G. H. Giurgea and A. T. H. Trutia, Spectrochim. Acta, 11, 441(1957).

5. R. Mavrodineanu and R. C. Hughes, Spectrochim. Acta, 19, 1309(1963).

6. C. David West and David N. Hume, Anal. Chem., 36, 413(1964).

7. S. Greenfield, I. L. Jones and C. T. Berry, Analyst, 89, 713(1964).

8. S. Greenfield, P. B. Smith, A. E. Breeze and N. M. D. Chilton, Anal. Chim. Acta, 41, 385(1968).

9. R. H. Wendt and V. A. Fassel, Anal. Chem., 37, 921(1965).

10. R. H. Wendt and V. A. Fassel, Anal. Chem., 38, 339(1966).

11. V. A. Fassel and G. W. Dickinson, Anal. Chem., 40, 249(1968).

12. G. W. Dickinson and V. A. Fassel, Anal. Chem., 41, 1021(1969).

13. Claude Veillon and Marvin Margoshes, Spectrochim. Acta, 23B, 503(1968).

14. C. Veillon and M. Margoshes, Spectrochim. Acta, 23B, 553(1968).

15. H. Goto, K. Hirokawa and M. Suzuki, Z. Anal. Chem., 225, 130(1967).

16. M. Yamamoto and S. Murayama, Spectrochim. Acta, 23A, 773(1967).

17. S. Murayama, H. Matsumo and M. Yamamoto, Spectrochim. Acta, 23B, 513(1968).

18. S. Murayama, Spectrochim. Acta, 25B, 191(1970).

19. A. J. McCormack, S. C. Tong and W. D. Cooke, Anal. Chem., 37, 1470(1965).

20. C. A. Bache and D. J. Lisk, Anal. Chem., 37, 1477(1965).

21. C. A. Bache and D. J. Lisk, Anal. Chem., 38, 783(1966).

22. C. A. Bache and D. J. Lisk, Anal. Chem., 39, 786(1967).

23. R. W. B. Pearse and A. G. Gaydon, "Identification of Molecular Spectra," Wiley, New York, 1963.

24. H. Fay, P. H. Mohr and G. A. Cook, Anal. Chem., 34, 1254(1962).

25. E. Z. Sauter, Naturforsch., 3A, 392(1948).

26. J. C. Sternberg and R. E. Poulson, J. Chromatog., 3, 306(1960).

27. J. H. Runnels and J. H. Gibson, Anal. Chem., 39, 1398(1967).

28. I. Kleinmann and V. Svoboda, Anal. Chem., 41, 1029 (1969).

29. J. Richter in "Plasma Diagnostics," W. Lochte-Holtgreven, ed., North-Holland Publishing Co., Amsterdam, 1968, Chapter 1.

30. Hans R. Griem, "Plasma Spectroscopy," McGraw-Hill, New York, 1964.

31. D. R. Bates, A. E. Kingston and R. W. P. McWhirter, Proc. Roy. Soc., Ser. A267, 297(1962).

32. D. R. Bates, A. E. Kingston and R. W. P. McWhirter, Proc. Roy. Soc., Ser. A270, 155(1962).

33. W. Lochte-Holtgreven in "Plasma Diagnostics," W. Lochte-Holtgreven, ed., North-Holland Publishing Co., Amsterdam, 1968, Chapter 3.

34. J. Richter, Z. Astrophys., 61, 57(1965).

35. R. W. P. McWhirter and A. G. Hearn, Proc. Phys. Soc., 82, 641(1963).

36. L. de Galan, R. Smith and J. D. Winefordner, Spectrochim. Acta, 23B, 521(1968).

37. G. H. Dieke and H. M. Crosswhite, J. Quant. Spectrosc. Radiat. Transfer, 2, 97(1962).

38. G. Traving in "Plasma Diagnostics," W. Lochte-Holtgreven, ed., North-Holland Publishing Co., Amsterdam, 1968, Chapter 2.

39. H. R. Griem, A. C. Kolb and K. Y. Shen, Phys. Rev., 116, 4(1959).

40. H. R. Griem, Phys. Rev., 128, 515(1962).

41. Richard H. Tourin, "Spectroscopic Gas Temperature Measurement," Elsevier, New York, 1966.

42. William L. Barr, J. Opt. Soc. Am., 52, 885(1962).

43. Kjell Bockasten, J. Opt. Soc. Am., 51, 943(1961).

44. B. S. Malone and W. H. Corcoran, J. Quant. Spectrosc. Radiat. Transfer, 6, 443(1966).

45. K. Goldman, Physica, 29, 1024(1963).

BIOGRAPHICAL SKETCH

Karen Fallgatter (nee Zacha) was born in Effingham, Illinois on April 15, 1941. She attended public schools in Altamont, Illinois and Teutopolis, Illinois and was graduated from Teutopolis High School in June, 1959. In June, 1963, she received the degree of Bachelor of Science from Lewis College in Lockport, Illinois. In September, 1963, she enrolled in the Graduate School of the University of Florida. She was awarded a Master of Science degree by the University of Florida in December, 1966. During her work toward the degree of Doctor of Philosophy, she has held graduate teaching and research assistantships in the Department of Chemistry.

Karen Fallgatter is married to Michael Byers Fallgatter.

This dissertation was prepared under the direction of the chairman of the candidate's supervisory committee and has been approved by all members of that committee. It was submitted to the Dean of the College of Arts and Sciences and to the Graduate Council, and was approved as partial fulfillment of the requirements for the degree of Doctor of Philosophy.

August, 1970

H. E. Spivey
Dean, College of Arts and Sciences

Dean, Graduate School

Supervisory Committee:

J. D. Winefordner
Chairman

J. H. [illegible]

C. A. Hooper

Roger G. Bates

R. J. Hanrahan